

# Noninvasive hemoglobin sensing and imaging: optical tools for disease diagnosis

Michaela Taylor-Williams<sup>ⓑ</sup>,<sup>a,b</sup> Graham Spicer,<sup>a,b</sup> Gemma Bale<sup>ⓑ</sup>,<sup>a,c</sup>  
and Sarah E. Bohndiek<sup>ⓑ</sup>,<sup>a,b,\*</sup>

<sup>a</sup>University of Cambridge, Department of Physics, Cavendish Laboratory, Cambridge,  
United Kingdom

<sup>b</sup>University of Cambridge, Cancer Research UK Cambridge Institute, Cambridge,  
United Kingdom

<sup>c</sup>University of Cambridge, Electrical Division, Department of Engineering, Cambridge,  
United Kingdom

## Abstract

**Significance:** Measurement and imaging of hemoglobin oxygenation are used extensively in the detection and diagnosis of disease; however, the applied instruments vary widely in their depth of imaging, spatiotemporal resolution, sensitivity, accuracy, complexity, physical size, and cost. The wide variation in available instrumentation can make it challenging for end users to select the appropriate tools for their application and to understand the relative limitations of different methods.

**Aim:** We aim to provide a systematic overview of the field of hemoglobin imaging and sensing.

**Approach:** We reviewed the sensing and imaging methods used to analyze hemoglobin oxygenation, including pulse oximetry, spectral reflectance imaging, diffuse optical imaging, spectroscopic optical coherence tomography, photoacoustic imaging, and diffuse correlation spectroscopy.

**Results:** We compared and contrasted the ability of different methods to determine hemoglobin biomarkers such as oxygenation while considering factors that influence their practical application.

**Conclusions:** We highlight key limitations in the current state-of-the-art and make suggestions for routes to advance the clinical use and interpretation of hemoglobin oxygenation information.

© The Authors. Published by SPIE under a Creative Commons Attribution 4.0 International License. Distribution or reproduction of this work in whole or in part requires full attribution of the original publication, including its DOI. [DOI: [10.1117/1.JBO.27.8.080901](https://doi.org/10.1117/1.JBO.27.8.080901)]

**Keywords:** hemoglobin; sensing; imaging; spectroscopy.

Paper 220074VR received Apr. 6, 2022; accepted for publication Jun. 27, 2022; published online Aug. 3, 2022.

## 1 Introduction

Optical-imaging biomarkers are defined characteristics measured with an optical imaging modality to indicate normal biological or pathological processes. Optical-imaging biomarkers can help researchers better understand disease development and give clinicians the ability to diagnose and treat diseases in patients.<sup>1,2</sup>

Based on the absorption of light by hemoglobin, optical imaging biomarkers such as hemoglobin concentration, oxygen saturation, and blood flow can be measured with a range of instruments for clinical disease evaluation. Hemoglobin is a protein in blood that transports oxygen to organs. Oxygen plays a vital role in cellular aerobic respiration, where it reacts with glucose to form adenosine triphosphate, water (H<sub>2</sub>O), and carbon dioxide (CO<sub>2</sub>), essential for maintaining

\*Address all correspondence to Sarah E. Bohndiek, [seb53@cam.ac.uk](mailto:seb53@cam.ac.uk)

healthy tissue and blood vessels. Hemoglobin oxygenation is often used as a vital sign; low oxygenation at the level of the organism can indicate a systemic disease, such as chronic obstructive pulmonary disease and apnea.<sup>3,4</sup> Poor oxygenation in a particular organ or tissue can be symptomatic of an insult due to injury or illness, such as diabetes, skin trauma, rheumatic disease, or cancer.<sup>1,5–8</sup>

Noninvasive, low-cost, safe, and portable methods based on optics for extracting hemoglobin-derived biomarkers have become vital tools in patient management that can be applied in real time at the bedside. Despite widespread use of methods such as pulse oximetry, the uptake of newer technologies that go beyond point measurements remains relatively limited; however, there are many promising tools in development, ranging from 3D volumetric imaging of vascular architecture to spatially-resolved functional images of tissue oxygenation. Being less expensive and more portable in general than conventional radiological imaging methods, these have the potential to impact patient care in a wide range of debilitating illnesses, ranging from rheumatoid and vascular diseases to neurodegenerative diseases and cancer.

Here, we review these noninvasive methods for quantifying hemoglobin-derived biomarkers, including pulse oximetry, as commonly used in clinical practice worldwide, together with promising tools emerging in the research setting for imaging. The relative strengths and weaknesses of different methods are considered according to the application, grouped by mode of operation, including single-point detection, superficial imaging (up to 1- to 2-mm depth); and deep tissue imaging. We compare techniques based on the technology used, analysis methods, and current research or clinical applications; we then highlight limitations that would benefit from future research.

## 2 Impact of Tissue Properties on Optical Measurement of Hemoglobin Biomarkers

### 2.1 *Biology of Human Blood*

Human blood consists of plasma (about 55 vol.%) and cells (~45 vol.%) in which 99% of the cells are red blood cells (RBCs) and the remaining 1% are leukocytes and thrombocytes.<sup>9,10</sup> Plasma is a complex composition of dissolved ions (electrolytes), lipids, sugars, and proteins.<sup>10</sup> RBCs, also known as erythrocytes, have a flat biconcave shape and a mean volume of 90  $\mu\text{m}^3$ ,<sup>9,11</sup> and they contain about 30 pg of hemoglobin, a globular metalloprotein responsible for oxygen transport throughout the body.<sup>9,11</sup> Hemoglobin concentrations range from 134 to 173 g/L in whole blood and 299 to 357 g/L in RBCs, varying according to age, gender, and health status. For example, anemia, cancer, or hereditary hemochromatosis decrease hemoglobin levels in the blood.<sup>9,12</sup>

Each hemoglobin molecule contains four heme groups that can be bound to oxygen; the unbound state is referred to as deoxygenated hemoglobin, Hb, and the saturated bound state is considered oxygenated and denoted by HbO<sub>2</sub>.<sup>10</sup> Sometimes the oxygen saturation of arterial blood, SaO<sub>2</sub>, is differentiated from that of peripheral blood, StO<sub>2</sub>, because arterial blood oxygenation should be the same throughout the body. In contrast, peripheral blood has varying oxygenation levels as oxygen is absorbed from the blood by peripheral systems.<sup>11,13,14</sup> Hemoglobin is also able to bind to other molecules forming carboxyhemoglobin, which arises during carbon monoxide inhalation;<sup>15,16</sup> sulfhemoglobin, which arises due to the irreversible binding of sulphur in the presence of sulfonamides;<sup>17</sup> and carbaminohemoglobin, which results from the binding of hemoglobin in venous blood to carbon dioxide.<sup>18</sup> A further variant state of hemoglobin is methemoglobin,<sup>19–21</sup> in which hemoglobin binds iron in the Fe<sup>3+</sup> state (unlike normal hemoglobin that binds Fe<sup>2+</sup>), which prevents the binding of oxygen. Methemoglobin occurs naturally in blood at ~1% to 2% concentration,<sup>15</sup> but it can be elevated due to side effects of medication or environmental factors.<sup>22</sup> Finally, genetic variants of hemoglobin, such as hemoglobin S, which causes sickle cell anemia, can influence hemoglobin structure and binding properties.<sup>23</sup> Myoglobin, a chromophore commonly found in muscles, binds oxygen with a higher affinity than hemoglobin.<sup>24</sup> Myoglobin has a similar spectral response to hemoglobin and may be found in the bloodstream following muscle injury.<sup>24,25</sup>

## 2.2 Optical Properties of Biological Tissue

Tissue is a complex turbid medium composed of different cell types and protein-rich extracellular matrix, which strongly impact the propagation of light.<sup>11,26,27</sup> Absorption is the transformation of light energy to some other form of energy, such as heat, sound or fluorescence, as light traverses tissue and is quantified by the absorption coefficient,  $\mu_a$  ( $\text{cm}^{-1}$ ). Absorption is the primary optical interaction that is exploited to measure hemoglobin biomarkers. In turbid media, scattering is a major contributor to light attenuation and can confound attempts to measure hemoglobin absorption because blood is a highly scattering liquid with strong anisotropy. Scattering refers to a change in the direction of light propagation and is quantified by the scattering coefficient,  $\mu_s$  ( $\text{cm}^{-1}$ ), together with directional factors such as the scattering phase function and anisotropy factor, which further relate to the tissue refractive index.

### 2.2.1 Optical properties of RBCs, hemoglobin, and its derivatives

The absorption coefficient of hemoglobin is a function of wavelength and the binding state (Fig. 1).<sup>32</sup> Hemoglobin is usually oxygen-bound, whereas other variants mentioned above can modify the absorption spectrum and should be considered if relevant to the pathology being assessed because they can confound the measurement.<sup>10,13,23,33,34</sup> It should be noted that the spectra of hemoglobin and its variety of physiologically relevant bound states are often measured after extracting the hemoglobin protein from RBCs, so they do not consider variation that arises due to scattering from different RBC geometries and orientations.

In the absence of shear stress, human RBCs are biconcave discs with a diameter of 7 to 8  $\mu\text{m}$ , maximal thickness of 2 to 3  $\mu\text{m}$ , and minimal thickness of 0.8 to 1.5  $\mu\text{m}$ .<sup>35,36</sup> Concentrations of Hb within an RBC are high, on the order of 300 to 360 mg/mL, and the total refractive index of the cell is well approximated by that of pure hemoglobin through the application of the Kramers–Kronig relations on the total absorption spectrum.<sup>37,38</sup> When light is incident upon a single RBC, scatter from the near and far membrane interfaces leads to a characteristic oscillatory scattering spectrum and phase function.<sup>36,39</sup> The oscillatory spectral shape makes oximetry of a single RBC impossible without *a priori* knowledge of the precise shape and orientation of the RBC; however, averaging over many cells with random orientation can smooth this oscillation, which permits measurement of oxygen saturation of RBCs in capillaries.<sup>39,40</sup> In addition, hematocrit, the volume fraction of RBCs in whole blood, the presence of blood plasma, and other factors affect the absorption spectra.<sup>18,41–44</sup>

The most common hemoglobin-derived optical imaging biomarkers are total hemoglobin (referred to as THb hereafter) and oxygen saturation (referred to as  $\text{sO}_2$  hereafter). THb is often evaluated using a single wavelength absorption measurement taken at an isosbestic point of

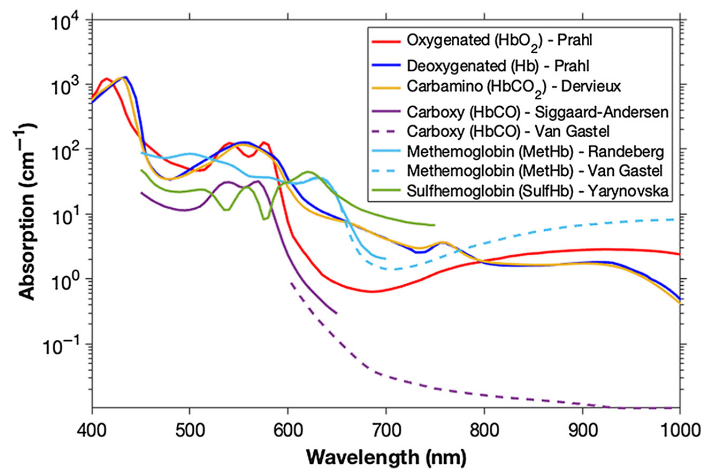


**Fig. 1** The optical absorption of hemoglobin and associated variants. Representative spectra are shown for oxygenated,<sup>28</sup> deoxygenated,<sup>28</sup> carbamino,<sup>18</sup> carboxy (visible<sup>29</sup> and NIR<sup>19,20</sup>), methemoglobin (visible<sup>30</sup> and NIR<sup>19,20</sup>), and sulfhemoglobin.<sup>31</sup>

HbO<sub>2</sub> and Hb (i.e., when their absorption coefficients are equal). sO<sub>2</sub> requires an absorption measurement to be made at multiple wavelengths (at least 2), usually spanning regions where either HbO<sub>2</sub> and Hb dominate the absorption properties. Data are then often analyzed by applying multivariate statistical approaches for spectral unmixing<sup>45</sup> to extract the sO<sub>2</sub> value. The absorption coefficients of HbO<sub>2</sub> and Hb are related through sO<sub>2</sub> to the overall optical absorption  $\mu_a$  as<sup>11,45</sup>

$$sO_2 = \frac{[HbO_2]}{[HbO_2] + [Hb]}, \quad (1)$$

$$\mu_a(\lambda) = c_{Hb} \left\{ \frac{sO_2}{100} \mu_{aHbO_2}(\lambda) + \left( 1 - \frac{sO_2}{100} \right) \mu_{aHb}(\lambda) \right\}, \quad (2)$$

where  $c_{Hb}$  is the concentration of hemoglobin in the tissue.

In addition to hemoglobin, many other molecules interact with light depending on their concentration and distribution throughout the tissue,<sup>46</sup> which can disrupt light propagation and also introduce spectral coloring at depth in tissue, confounding attempts to measure THb and sO<sub>2</sub>. Furthermore, the scattering and refractive index properties of blood are affected by hemoglobin concentration, erythrocyte volume, shape, and aggregation, each of which can be modified in disease. Unlike the absorption coefficient, the anisotropy and the scattering coefficients of blood are not dependent on the changes in oxygenation.<sup>9,47</sup>

Hemoglobin-derived biomarkers often rely on variations in the absorption or scattering by hemoglobin molecules or RBCs, and the hardware used to make these measurements varies, including the use of LEDs or lasers for illumination with optical sensors (both arrays and point sensors) or ultrasound sensors for detection. The methods described in this review are summarized in Table 1.

### 3 Point Sensing of Hemoglobin sO<sub>2</sub> through Pulse Oximetry

Pulse oximetry makes a localized measurement of arterial hemoglobin sO<sub>2</sub>. To make this measurement, the absorption of tissue is evaluated at two or more different wavelengths, selected according to where the absorption coefficients of Hb and HbO<sub>2</sub> differ sufficiently for their ratio to be evaluated as a biomarker that can be correlated directly to sO<sub>2</sub> [Eq. (1)].

#### 3.1 Clinical Applications and Research Studies

Pulse oximetry has been extensively reviewed elsewhere.<sup>13,48,49,135,136</sup> Pulse oximetry is deployed in many medical applications, from at-home first aid to clinical intensive care units and surgical theaters<sup>13</sup>, and it has found particular utility in assessing hypoxemia in COVID-19 patients<sup>137</sup> as nonspecialists with minimal training can efficiently operate pulse oximeters.<sup>49,138</sup> Pulse oximetry research in the clinic focuses on its use in treating and diagnosing diseases, such as optimizing oxygenation of ventilated patients, screening neonates for congenital heart diseases, and monitoring patients with sleep apneas.<sup>50,51,139,140</sup> Despite widespread use, it is also well established that pulse oximetry can suffer racial bias, which results in less accurate oxygenation readings for patients with more skin melanin content, a trait associated with darker skin. The impact of such bias is severe as it has been shown to result in less adequate medical treatment of such patients, meaning that it is important for clinicians to be aware of this limitation and it is also an important area for future research and development.<sup>141,142</sup> Although this bias has been well known for some time, it has been increasingly studied as a result of COVID-19 and the increased clinical use of pulse oximeters to treat respiratory conditions.

#### 3.2 Technology

Light absorption in pulse oximetry is typically measured using alternating illumination by LEDs at two different wavelengths.<sup>135,143,144</sup> Because the wavelength of the illuminating light is altered with time, oxygenation measurements are susceptible to motion artifacts, which change the area

**Table 1** Overview of noninvasive hemoglobin monitoring and imaging.

Technology	Clinical application(s)	Spatial resolution	Benefits	Limitations	Clinical status and future potential	References
<b>Pulse oximetry</b>	Used to identify hypoxemia in a range of healthcare settings.	Single point measurement with no spatial resolution.	<ul style="list-style-type: none"> <li>•Real-time monitoring of arterial saturation.</li> <li>•Extremely simple and quick to use in a clinical setting.</li> <li>•It can be used at the patient's bedside.</li> </ul>	<ul style="list-style-type: none"> <li>•Single point location measurement. It can be inaccurate due to calibration assumptions</li> <li>•Errors are associated with variations in hemoglobin and poor perfusion on the tissue measured.</li> </ul>	Commonly used in primary through to tertiary care. Potential for increased deployment at-home through wearables and low-cost devices.	13,48–59
<b>Nailfold capillaroscopy</b>	Diagnosing and monitoring systemic scleroderma and other arthritic conditions.	Spatial resolution varies from 0.1 to 10 $\mu\text{m}$ laterally dependent upon the imaging NA, with corresponding imaging focal depth (Rayleigh range).	<ul style="list-style-type: none"> <li>•Real-time imaging of capillaries and blood flow is relatively easy.</li> <li>•Typically, the design is portable, so it can be used at the bedside if needed.</li> </ul>	<ul style="list-style-type: none"> <li>•Lack of standardization around the quantification of capillary parameters.</li> <li>•Measures only structural, not functional, information about the capillaries.</li> <li>•Restricted to only imaging the nailfold capillaries.</li> </ul>	Used in tertiary care. Emerging methods include quantification of blood flow, blood cell counts, and oxygenation imaging.	5,60–70
<b>Spectral reflectance imaging (MSI and HSI)</b>	Narrowband endoscopic imaging.	Spatial resolution varies from 5 to 400 $\mu\text{m}$ depending on the application because most systems use lenses for magnification. Reflectance signal restricted to superficial to 200 $\mu\text{m}$ of tissue due to scattering.	<ul style="list-style-type: none"> <li>•A versatile method that can image multiple hemoglobin biomarkers as well as other proteins of interest.</li> <li>•Relatively high spatial resolution is possible.</li> </ul>	<ul style="list-style-type: none"> <li>•Processing of images can be complicated and is not always possible in real time</li> <li>•Snapshot methods are fast but sacrifice spectral and spatial resolution</li> <li>•Scanning methods are slow but have a higher spectral resolution.</li> </ul>	Commonly used in tertiary care for endoscopic surveillance. Otherwise, used in research and small-scale clinical trials with promising applications in cancer detection, skin lesions, e.g., burns, and surgical tissue health.	2,6,8,30, 71–85
<b>PAI</b>	Breast lesion evaluation.	PAM can have a spatial resolution of $\sim 30 \mu\text{m}$ with an imaging depth of around 2 to 6 mm. PAT can have a resolution of $\sim 200 \mu\text{m}$ with a penetration depth 2 to 3 cm.	<ul style="list-style-type: none"> <li>•Can assess the relative hemoglobin saturation together with other biomarkers at depth while maintaining a reasonable spatial resolution.</li> <li>•It is a versatile technique scaling spatial resolution with depth of imaging required.</li> </ul>	<ul style="list-style-type: none"> <li>•Trade-off between resolution and depth.</li> <li>•Requires acoustic contact between the tissue and detectors.</li> <li>•Systems can be costly, though LEDs can be used at the expense of imaging quality.</li> <li>•The use of high-power pulsed light can present additional safety considerations to ensure that stray light does not damage patients or clinicians' eyes</li> </ul>	Large scale clinical trials ( $n > 2000$ ) for the diagnosis of breast cancer. Small scale clinical trials or proof of concept for other applications, such as severity assessment in Crohn's disease and dermatological conditions.	32,86–109

**Table 1 (Continued).**

Technology	Clinical application(s)	Spatial resolution	Benefits	Limitations	Clinical status and future potential	References
<b>Spectroscopic OCT</b>	Structural OCT is a clinical standard of care for retinal imaging. Spectroscopic OCT not yet clinically approved.	Lateral resolution determined by illumination optics, typically tens of $\mu\text{m}$ but as low as 1 to 2 $\mu\text{m}$ is achievable. Axial resolution determined by source/detector bandwidth, on the order of tens of $\mu\text{m}$ down to 1 $\mu\text{m}$ . Penetration depth is limited to $\sim 1$ mm in medium-scattering tissue.	Real-time tomographic imaging with high resolution ideal for resolving tissue layers, structural characteristics in 3D.	<ul style="list-style-type: none"> <li>Optical scattering in tissue limits imaging depth to 1 to 2 mm for most tissues.</li> <li>Laser scanning of sample introduces potential for motion artifacts in image, ophthalmic visible OCT implementation limited by safety threshold and patient aversion.</li> </ul>	Structural OCT widely used in primary and tertiary centers for ophthalmology, dermatology, and dentistry, also in tertiary centers for cardiology. Spectroscopic OCT for oximetry in preclinical development.	39, 110–122
<b>DOI or NIRS</b>	Assessment of brain activity (fNIRS or DOT). Monitoring of tissue oxygenation (cerebral oximetry/ NIRS).	1 to 30 mm spatial resolution; high resolutions are only possible at shallow imaging depths ( $< 2$ cm). Low-resolution imaging is possible up to 10 cm into the tissue.	Capable of determining blood oxygenation in tissue and other chromophores such as melanin, lipids, cytochrome-c-oxidase, and water.	<ul style="list-style-type: none"> <li>Relatively low resolution; obtaining high resolution requires prior knowledge of tissue composition and a high density of optodes.</li> <li>DOI techniques may be combined with other imaging modalities such as MRI or ultrasound to assess tissue composition, resulting in increased system cost.</li> <li>Computationally-intensive and time-consuming, resulting in limited real-time imaging (spectroscopy does not have this problem).</li> </ul>	Clinical approval and small-scale clinical use of tissue oximetry/NIRS for assessment of brain oxygenation. fNIRS/DOT used commonly as a research tool to monitor brain activity. Small scale clinical trials or proof of concept for other applications, such as breast cancer diagnosis, and joint inflammation.	123–134

of tissue being illuminated and coupling to the tissue, resulting in inaccuracies. Commonly used wavelength pairs are 660 and 940 nm or 665 and 894 nm,<sup>13,52–55</sup> which are applied in two different modes.

- **Transmission:** Tissue such as the finger, toe, or earlobe is illuminated, and the light transmitted through the tissue is detected by a sensor to determine the amount of light attenuated by the tissue [Fig. 2(a)].
- **Reflection:** Tissue such as the finger, foot, or forehead is illuminated, and the amount of light reflected by the tissue and underlying bone is detected by a sensor and used to determine the amount of light that the tissue has absorbed. Reflection pulse oximetry tends to

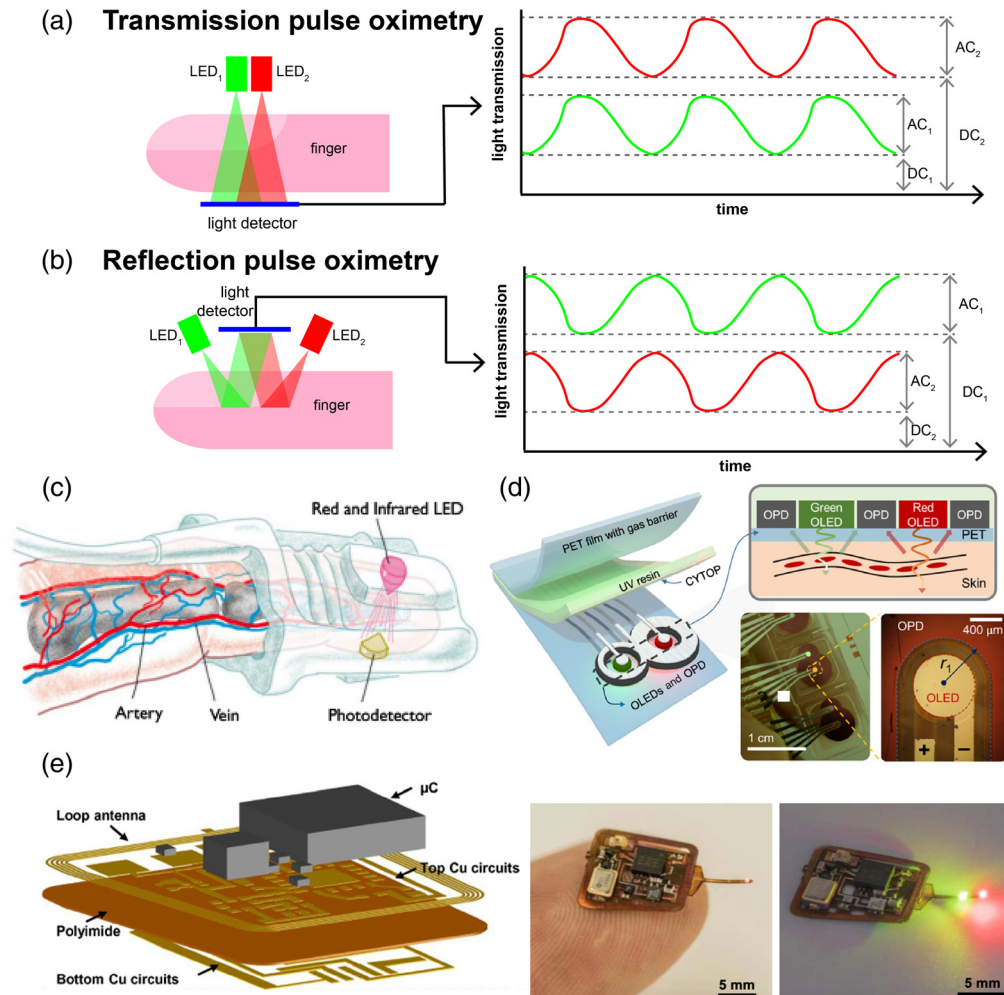


**Fig. 2** Pulse oximetry. Schematic illustration of pulse oximetry in the two different operation modes: (a) transmission and (b) reflection. The detected light is cyclic due to the pulsatile nature of blood in the peripheral vascular system. Both transmission and reflection modes have alternating components (AC) and direct components (DC). In tissue, the transmission and reflection of light vary based on the changes in absorption due to blood volume and oxygenation. That is  $R + A + T \approx 1$ , when  $R$ ,  $A$ , and  $T$  are the normalized reflection, absorption, and transmission intensities, respectively. For this reason, in reflection pulse oximetry, the peak intensity of light will be off by half a cycle from that of the transmission cycle. Examples of pulse oximeter devices include (c) transmission-based devices widely used in a clinical setting. Reproduced with permission from Ref. 145. (d) Low-power devices in development that adhere to the skin and use flexible OLED illumination. Reproduced with permission from Ref. 51. (e) Battery-free pulse oximeters in development that use near field communication for power. Reproduced with permission from Ref. 146.

have a higher signal when there is low perfusion.<sup>13,147</sup> In reflection pulse oximetry, it can be challenging to isolate the light that has gone deeper into tissue from light that has been scattered or reflected at the surface of the tissue [Fig. 2(b)].

Evolving from the traditional fingertip pulse oximeters [Fig. 2(c)], the current development of the technology mainly targets wearable devices and focuses on low power usage [Fig. 2(d)], optimization of signal detection, reduction of motion artifacts, flexible illumination and detection [Fig. 2(e)], low-cost devices, miniaturization, and calibration techniques.<sup>51,56–59</sup>

### 3.3 Analysis

The theory of oximetry analysis has been extensively reviewed by Mackenzie and Harvey,<sup>148</sup> so it will be only briefly introduced; readers are referred to the prior review for a more detailed description. The total extinction coefficient for blood is denoted as  $\epsilon$  and related to  $\text{SaO}_2$  as<sup>13</sup>

$$\epsilon = \epsilon_O \text{SaO}_2 + \epsilon_D (1 - \text{SaO}_2). \quad (3)$$

Further analysis of the extinction coefficient is needed to isolate the signal from arterial blood because venous blood also absorbs the light, along with other chromophores that appear in the light path, such as melanin (in the skin). It is possible to exploit the cyclic nature of the extinction coefficient due to the pumping of blood by finding the ratio of the variable component (AC) and constant component (DC) at two different wavelengths [Figs. 2(a) and 2(b)], where the difference in light absorption is rather large<sup>13,48,135</sup>

$$R = \frac{(\text{AC}/\text{DC})_1}{(\text{AC}/\text{DC})_2}. \quad (4)$$

The ratio  $R$ , also known as the modulation ratio, is then related to  $\text{SaO}_2$  through a calibration procedure using best-fit analysis according to the equation

$$\text{SaO}_2 = a + bR, \quad (5)$$

where the variables  $a$  and  $b$  are calculated for each device during testing, based on a linear regression between the modulation ratio and the  $\text{SaO}_2$  value.<sup>135,149</sup> Calibration was originally performed with human volunteers, changing  $\text{SaO}_2$  values by limiting the oxygen in the air that they breathed from 70% to 100%  $\text{SaO}_2$ , which determined the  $R$  values.<sup>150</sup> These are valid across devices with the same design, which means that individual devices did not have to be calibrated. Calibration techniques have evolved, so volunteers are no longer required. For example, several devices simulate the circulatory system and finger using pumps to mimic the pulsatile flow of arterial blood and venous blood.<sup>12,151–155</sup> The system is then sealed off, and the oxygenation of the blood can be controlled by varying the oxygen content of the system. Alternatives include electrical simulators that emit light from an LED corresponding to the light detected by the sensor to mimic the light transmitted in a typical finger. This technique requires prior knowledge of the pulse oximeter being calibrated. Once in operation, pulse oximeters are rarely recalibrated.<sup>150</sup>

### 3.4 Limitations

Pulse oximetry measurements typically have an error of 3% to 4% depending on the device and calibration used, which is actually sufficient to impact patient care in some cases.<sup>150,156</sup> In addition, standard pulse oximeters cannot detect the presence of methemoglobin, carboxyhemoglobin, or hemoglobin mutations, although their presence and concentrations outside of the expected range will affect the oxygenation readings.<sup>15,23</sup> Some targeted pulse oximeters are able to detect methemoglobin and carboxyhemoglobin, but they are usually used in specific scenarios in which high levels of these derivatives are expected due to exposure.<sup>157</sup> Hemoglobin  $F$ , present in fetuses and infants under 6 months, has a greater oxygen affinity, which allows the fetus to absorb oxygen from the mother's bloodstream;<sup>10</sup> in infants, its presence can increase the error in

pulse oximetry by a further 3% in addition to the typical errors.<sup>13</sup> Additionally, when there is poor perfusion to tissues, pulse oximetry can be limited, and if there is not a significant pulse detected, the technique will have increased inaccuracies.<sup>55</sup> Finally, pulse oximetry has been found to suffer racial bias in two large cohorts, in which black patients had nearly three times the frequency of occult hypoxemia not detected by pulse oximetry as white patients.<sup>141,142</sup> Skin pigmentation leads to an overestimation of arterial oxygen saturation in dark-skinned individuals, which could seriously impact medical decision making and long-term outcomes.<sup>158</sup> These limitations merit increased attention in research and development given the potential for long-term and widespread use of pulse oximetry in COVID-19 patient management and the interest in deployment of the technology in the wearable setting.

#### 4 Reflectance Imaging of Hemoglobin

Optical imaging of hemoglobin biomarkers requires the operator to build a spatially resolved map of hemoglobin absorption at multiple wavelengths, again exploiting the differential absorption coefficients of Hb and HbO<sub>2</sub>.<sup>26,71,159</sup> Several methods can be used to achieve this, including point-scanning spectroscopy, multispectral imaging, and hyperspectral imaging [Fig. 3(a)]. The result is a 3D dataset  $((x, y, \lambda))$ <sup>26,72,159,163</sup> that can be subjected to multivariate analysis methods to extract from the measured spectra the concentrations of their contributing chromophores (e.g., Hb and HbO<sub>2</sub>), referred to as “endmembers” for unmixing.<sup>26,72,164–167</sup> From these multivariate analyses, biomarkers that relate to THb and sO<sub>2</sub> can then be extracted.

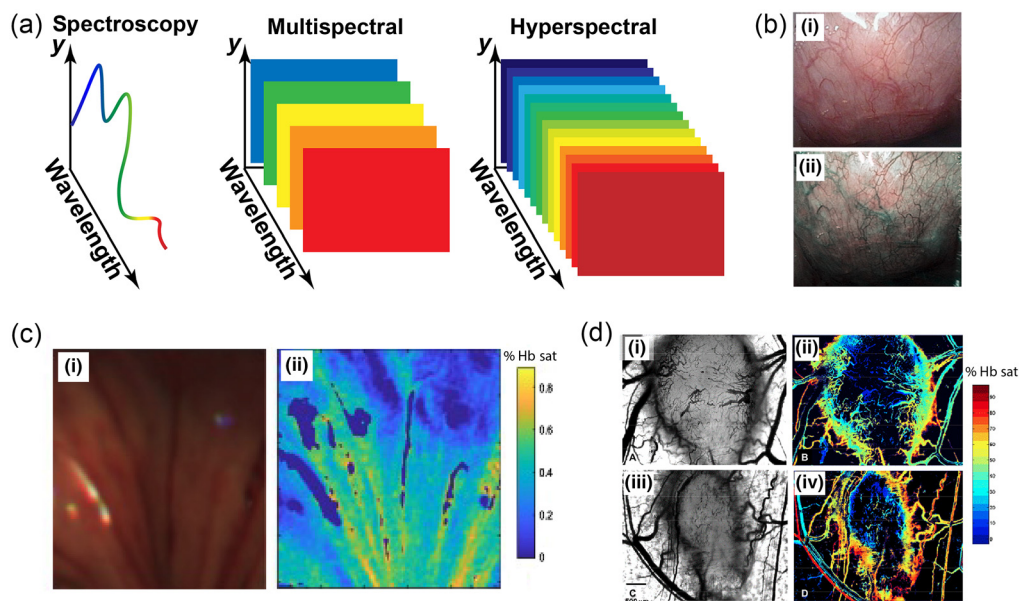


**Fig. 3** Spectral reflectance imaging. (a) Overview of spectral reflectance imaging methods.<sup>159</sup> Point-scanning spectroscopy can be used to build spectral information using a standard spectrometer. Alternatively, a spectral camera can be used to collect either a limited number of wavelengths (multispectral, typically <10 spectral bands) or a more continuous spectrum (hyperspectral). (b) Endoscopy images of the esophagus with (i) RGB imaging and (ii) narrowband imaging, which improves the contrast of the blood vessels. Reproduced with permission from Ref. 160. (c) Endoscopy of a porcine esophagus to determine tissue viability with 24 spectral bands from 460 to 690 nm (spectral resolution of 10 nm) using a slit hyperspectral imaging and fiber bundle probe and the resulting (i) reconstructed RGB image and (ii) unmixed oxygenation. Reproduced with permission from Ref. 161. (d) Hypoxia of tumors can be imaged using a liquid crystal tunable filter in conjunction with a CCD; this is demonstrated in mouse tumors; (i) and (iii) light microscopy of tumor vasculature in a dorsal skin window chamber, and the additional information of hemoglobin saturation is shown in (ii) and (iv) illustrating low oxygen saturation of the tumors. Reproduced with permission from Ref. 162.

#### 4.1 Clinical Applications and Research Studies

A widespread application of reflectance hemoglobin imaging is in gastrointestinal endoscopy. Virtual chromoendoscopy methods adapt the light source of the endoscopy to focus on two wavelength bands (415 and 540 nm), where hemoglobin absorbs strongly (Fig. 1), thus providing a high contrast morphological image of the tissue vasculature to the clinician.<sup>2,168</sup> Narrowband imaging is the most widely established of these methods and meets the ASGE thresholds for targeting biopsies when imaging patients with Barrett's esophagus for early signs of cancer.<sup>169</sup> More recently, clinical research studies have demonstrated that, by expanding the number of wavelengths captured in endoscopy,<sup>72,73,170</sup> it is possible to derive hemoglobin biomarkers of THb and sO<sub>2</sub> from spectral information to classify disease status;<sup>171</sup> however, further clinical study is needed to demonstrate efficacy.

Capillaroscopy is another reflectance-based imaging technique; it is used to image the blood vessels in the finger nailfold to diagnose disease, particularly to identify rheumatic diseases such as systemic scleroderma. Capillaries are microblood vessels from which oxygen and other nutrients are exchanged with the surrounding cells. In the finger nailfold, the capillaries are oriented in loops parallel to the skin, allowing for full visualization at high resolution in reflectance imaging mode. Capillary walls, formed from a single layer of endothelial cells lining the vessels, can rarely be detected during capillaroscopy, whereas the RBC column is visible, and morphological features associated with the capillary can be measured using monochrome, narrowband, and RGB imaging.<sup>60</sup> Capillary blood flow in the finger ranges in velocity from 0.67 to 4 mm/s depending on physiological factors and the cyclic nature of perfusion.<sup>172–174</sup> Morphological dysfunction of the capillaries is easily identified using the current techniques, but current methods do not make oximetry measurements related to this dysfunction.

Reflectance-based oximetry imaging has been widely explored in retinal imaging because the retina is one of the most metabolically active tissues in the human body.<sup>175</sup> Commercial retinal oximeters are applied to fundus cameras and use dual-wavelength illumination, akin to pulse oximetry, to acquire images simultaneously at one isosbestic wavelength and one sensitive to HbO<sub>2</sub>. Abnormal retinal oxygenation has been shown to detect diabetic retinopathy, age-related macular degeneration, and glaucoma.<sup>74,75,176</sup> In addition, the retina has similar vascular properties to the brain, making it a perfect window for understanding and diagnosing neurological disease in addition to ocular disease.<sup>75</sup> Nonetheless, retinal oximetry has yet to find routine clinical application, limited primarily by the impact of fundus pigmentation and vessel size on quantification.<sup>75</sup> Although some hyperspectral imaging technologies have been explored in an attempt to overcome these limitations, to the best of our knowledge, they have not found clinical application.

In smaller scale studies, clinical trials of reflectance-based hemoglobin imaging have been applied in areas from the skin to the brain. For example, the hemodynamic response of the human cortex has been visualized during open-cranium surgery using hyperspectral imaging combined with multivariate analysis.<sup>76</sup> Evaluation of hemoglobin oxygenation and melanin content in the face has been of interest for dermatological treatments such as the detection of skin cancer, assessment of scar healing, and evaluation of skin thickness.<sup>177–180</sup> Spectral imaging of hemoglobin in burns,<sup>8</sup> wounds,<sup>6</sup> and bruises<sup>30,77</sup> has been explored to assess the progress of healing in a quantitative manner. Moreover, spectral imaging of tissue sO<sub>2</sub> has found application in intraoperative imaging.<sup>161,181</sup> Postoperative imaging can also provide clinicians with information on how tissue is healing such as following breast reconstruction in which water, hemoglobin concentration, and oxygen saturation are key indicators for tissue perfusion, an important factor in recovery.<sup>182</sup>

#### 4.2 Technology

The simplest imaging oximetry methods include two or three wavelengths akin to pulse oximetry, which can be applied using sequential illumination by the target wavelength bands and imaging with a single camera or simultaneous illumination of all wavelengths (e.g., with broadband illumination) and capture using a spectrally resolved method, such as image splitting through band pass filters applied in front of two cameras. Expanding the spectral range of wavelengths to

capture more spectral features of Hb or HbO<sub>2</sub> (in the visible but also near-infrared range<sup>183</sup>) requires more complex hardware.

There are three main types of multi or hyperspectral systems used in medical imaging that can be applied for unmixing oxygenation of tissue.<sup>78,79,159</sup> In spatial scanning, a spectrograph records the spectral dimension ( $\lambda$ ) while being scanned across a sample. A one-dimensional spectrograph may be point-scanned or a two-dimensional (2D) spectrograph may be line scanned. The approach sacrifices temporal resolution and hence requires minimal movement of the sample to avoid motion artifacts. In spectral scanning, a 2D camera records the spatial dimensions ( $x, y$ ), while the spectral dimension is scanned, e.g., by changing the illumination wavelength or by filtering the imaging light path (e.g., with a filter wheel or tunable filter). This also has a scanning time associated with it, so it requires minimal movement to prevent spectral artifacts.

Finally, in snapshot methods, a system outputs spectral and spatial dimensions ( $x, y, \lambda$ ) simultaneously without scanning.<sup>78,79</sup> Snapshot systems may use beam splitting with dichroic filters, volume holographic optical element splitters, image replicating spectrometers, or multi-spectral filter arrays in the imaging path. Snapshot methods avoid motion artifacts, which makes them an exciting prospect for clinical application; however, they often exhibit poor optical efficiency. They also require a trade-off between spatial and spectral resolution, although this is less problematic for hemoglobin measurements, in which the target spectra are well characterized, and extensive evidence exists for the application of optical measurements. Nonetheless, optimization of the target wavelengths for snapshot imagers can substantially improve their performance.<sup>166,184–187</sup>

In addition to these intensity-based imaging methods, spatial frequency domain imaging (SFDI) can be used to interrogate hemoglobin-related biomarkers by exploiting modulated illumination of the tissue. SFDI typically uses sinusoidal patterns and extracts the demodulation of these patterns reflected from tissue to calculate absorption and scattering properties;<sup>123,188</sup> low frequencies are more sensitive to absorption whereas high frequencies are more sensitive to scattering.<sup>123</sup> Multiwavelength illumination<sup>189</sup> can then be used to calculate hemoglobin content and oxygenation,<sup>190,191</sup> e.g., in monitoring of peripheral circulation and vascular diseases,<sup>192</sup> for which there are FDA-cleared devices, as well as ulcers,<sup>193</sup> burns,<sup>194</sup> or tumor margin detection.<sup>195,196</sup> SFDI provides relatively high-resolution images, but conventional methods can be sensitive to motion artifacts<sup>188</sup> and computational processing can limit the rate of image display. More recent reports have shown that it is possible to overcome these limitations using single snapshot of optical properties methods, which can achieve video-rate imaging.<sup>197</sup>

### 4.3 Analysis

Two- or three-wavelength imaging methods may be viewed qualitatively and interpreted by the operator, as in narrowband imaging, or processed to output quantitative THb or sO<sub>2</sub> biomarkers in a manner similar to pulse oximetry, through calculation of image ratios and calibration of the results. For spectral imaging methods, analysis can be time-intensive due to the large amount of data collected, which can be problematic for clinical translation in which the real-time display of biomarker data is often desired. Analysis methods vary depending on the biomarkers targeted and the type of tissue imaged from the simplest techniques such as linear spectral unmixing<sup>198,199</sup> to more complex methods such as multivariate analysis and machine learning.<sup>26,72,164,165</sup> Linear spectral unmixing determines the type and concentration of chromophores present based on input reference spectra for oxy and deoxy hemoglobin, from which oxygen saturation can be calculated.<sup>76,170,200,201</sup> Spectral signatures can also be used directly in classification of disease status, e.g., cancer.<sup>171,181,202,203</sup> Sometimes, a combination of classification and unmixing techniques can produce the optimal results, allowing for data corrections to be applied in certain tissue types.<sup>26,76,166,170</sup> Similar methods are also used in depth-resolved imaging, but data may need to be corrected based on the imaging depth and the associated level of optical absorption and scattering. Machine learning methods have shown promise in this regard, enabling more accurate determination of hemoglobin oxygenation, particularly at depth, than classic linear spectral unmixing.<sup>204</sup>

#### 4.4 Limitations

Imaging tools for the assessment of hemoglobin can be subject to the same limitations as pulse oximetry. In addition, constraints that presently prevent clinical adoption of reflectance-based spectral imaging include cost, reliability of THb and sO<sub>2</sub> measurements, clinical evidence for sensitivity and specificity of THb and sO<sub>2</sub> in the diseases shown to be of interest in small-scale studies, and the need to process data in real time.<sup>2,71,167</sup> These challenges are common in the clinical translation of optical imaging biomarkers,<sup>2</sup> though fortunately, in the case of hemoglobin biomarkers, many devices have already navigated the pathway to the clinic, enabling initial studies to be undertaken.

### 5 Depth-Resolved Imaging

A key limitation of pulse oximetry and reflectance-based imaging is their inability to provide depth-resolved imaging of hemoglobin biomarkers. Two modalities are available to determine THb and sO<sub>2</sub> in tissue up to and beyond depths of 1 cm: photoacoustic imaging (PAI) and diffuse optical imaging (DOI); both have been evaluated in clinical trials and are at different stages of clinical adoption. PAI exploits the generation of acoustic waves by the absorption of pulsed light by hemoglobin to create deep tissue volumetric maps using pulsed illumination and ultrasound detectors [Fig. 4(a)].<sup>86–88</sup> DOI measures the properties of light scattering in tissue to generate absorption maps using synchronized illumination and photodiode-based detection [Fig. 4(b)].<sup>124–126</sup> At more restricted depths, below 1 cm, spectroscopic optical coherence tomography (OCT) is also applicable, combining broadband illumination with spectrally-resolved interferometric detection. Although these methods have been widely explored in the clinical research setting, they are only just beginning to find routine application in the clinic for patient management.

#### 5.1 Photoacoustic Imaging (PAI)

##### 5.1.1 Clinical research studies

By far, the most explored clinical PAI application is human breast cancer detection, extensively reviewed elsewhere,<sup>208,209</sup> due to the enhanced angiogenesis of breast cancers compared with background breast parenchyma and the scalability of PAI geometry allowing for a broad view of the area [Fig. 5(a)].<sup>86,89,208,209,213,214</sup> Multicenter clinical trials have recently been concluded covering >2000 women; these established the ability of PAI to increase the specificity of ultrasound imaging using a real-time map of relative Hb and HbO<sub>2</sub>.<sup>213,215</sup> PAI has also been explored in other cancer types, considering that neoangiogenesis is a hallmark of cancer, including thyroid,<sup>216</sup> prostate,<sup>215</sup> and melanoma among, others.<sup>217</sup> Beyond applications in cancer, PAI has found a wide range of potential applications in which depth-resolved information is required, e.g., in endoscopic procedures;<sup>90,91</sup> for evaluation of inflammation, such as arthritic joints,<sup>88,92</sup> foot ulcers,<sup>93</sup> and Crohn's disease;<sup>218</sup> vascular imaging;<sup>94</sup> and for the guidance of interventional procedures, such as in fetal placentas.<sup>95</sup>

##### 5.1.2 Technology

Pulsed illumination is required to excite PAI signals. Typically, tunable pulsed lasers with nano-second pulse durations have been used; however, pulsed laser diodes and LEDs have emerged recently as viable alternatives.<sup>219</sup> The generated acoustic waves are detected by ultrasound transducers, which may be single-element, linear, or curvilinear arrays or in a spherical arrangement, depending on the system's geometry. The type of transducer and associated center frequency or bandwidth is usually governed by the application, depending on the absorber size, laser pulse width, and required imaging depth.<sup>220</sup> PAI can be deployed in different geometries, including tomography, mesoscopy, and microscopy. Tomography systems have found the most widespread clinical application as they provide an adequate field of view and spatial resolution for imaging of hemoglobin in deep tissue such as the breast; mesoscopy systems have also been applied

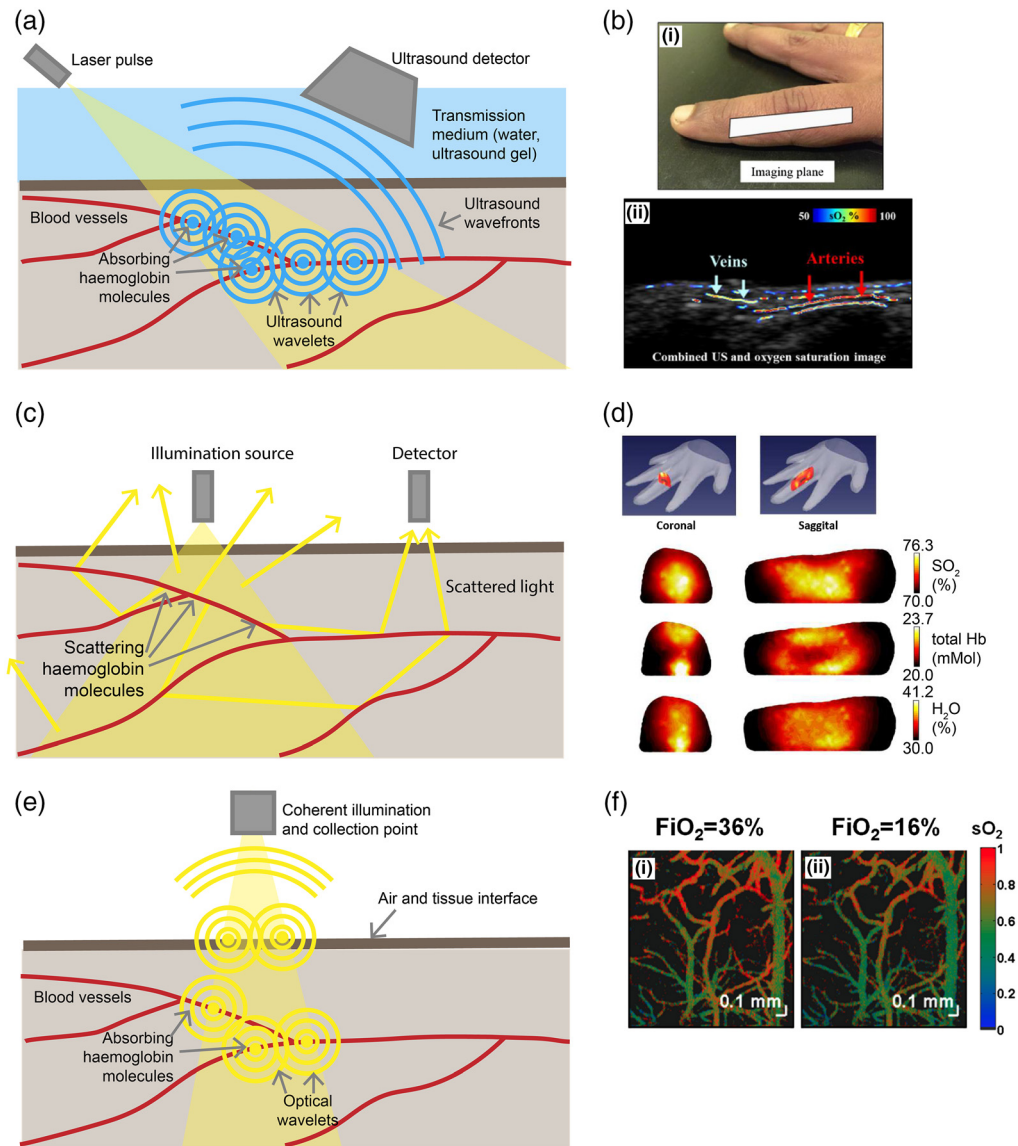


**Fig. 4** Principles of depth-resolved imaging. (a) In photoacoustic imaging, the absorption of light pulses generates a broadband acoustic wave detected at the tissue surface by an ultrasound transducer. (b) Photoacoustic imaging of oxygenation of the finger in combination with ultrasound to image the veins and arteries. Reproduced with permission from Ref. 205. (c) In DOI (and DCS techniques), illuminated light is scattered in tissue collected by an offset optical detector at the tissue surface. (d) DOI data acquired from the human finger is processed to quantify oxygenation, hemoglobin concentration, and water. Reproduced with permission from Ref. 206. (e) In OCT, coherent light illuminates the tissue, and the light that reflects at interfaces is collected and combined with a reference arm, so interference occurs; from this interference, depth-resolved images of the absorption and scattering properties of tissue can be resolved. (f) Oxygen resolved spectroscopic OCT on mice brains illustrating how the fraction of inspired oxygen ( $FiO_2$ ) affects the oxygenation of the arteries and veins in the brain. Reproduced with permission from Ref. 207.

clinically to visualize vascular network architectures in the skin given their limited penetration depths.<sup>221</sup>

### 5.1.3 Analysis

The acoustic wave generated in response to pulsed optical illumination depends on the absorption properties of tissue according to

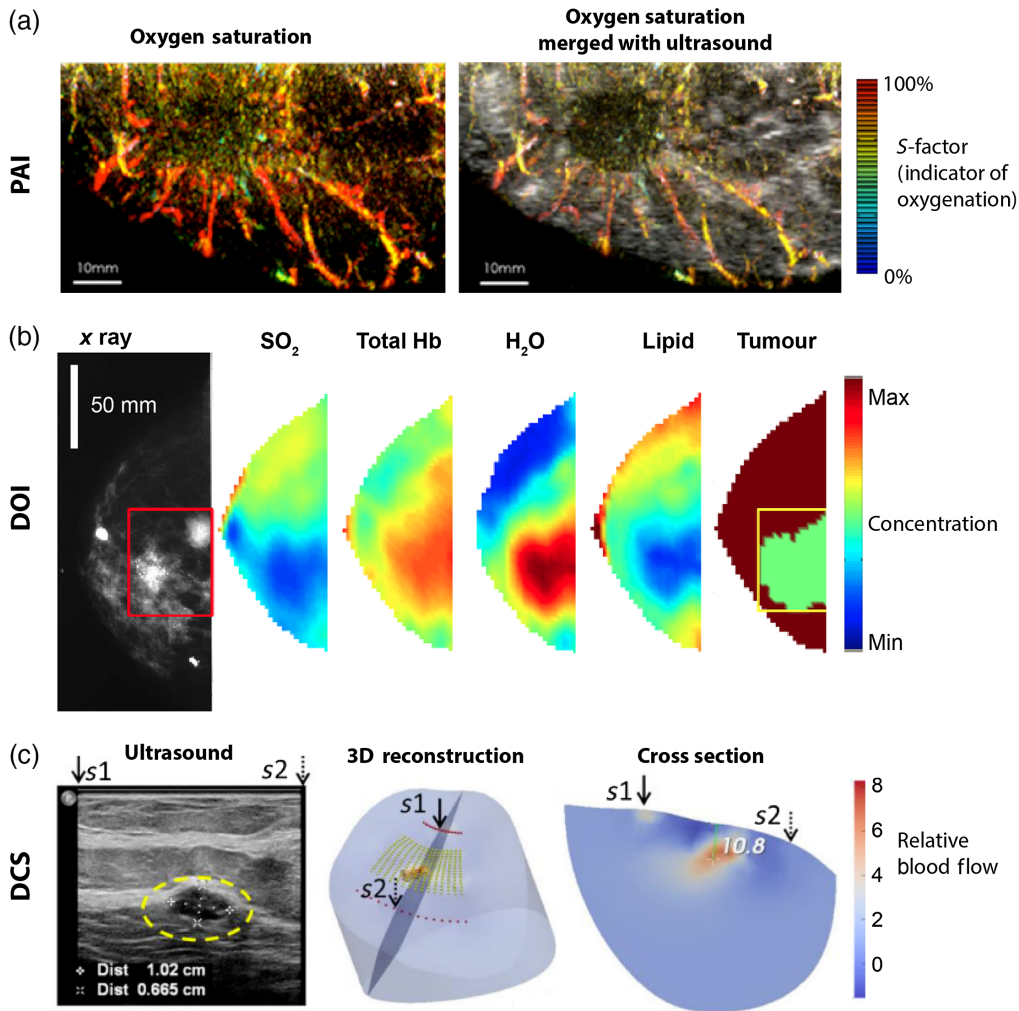


**Fig. 5** Tomographic imaging of the human breast for cancer detection (a) PAI of sO<sub>2</sub> in breast with infiltrating ductal carcinoma (IDC); S-factor was defined to account for system accuracy and fluence compensation. Reproduced with permission from Ref. 210. (b) DOI of breast IDC (indicated by the red box) resolves sO<sub>2</sub>, THb, H<sub>2</sub>O, lipid, concentrations of which serve to highlight the tumor. Reproduced with permission from Ref. 211. (c) DCS of blood flow relative to an ultrasound image of low-grade carcinoma; the tumor is circled in yellow. These images are referenced to positions s1 and s2 to compare the ultrasound, 3D reconstruction, and cross-section. Reproduced with permission from Ref. 212.

$$p_0(z) = \Gamma \mu_a F_0 e^{-\mu_0 z}, \quad (13)$$

where  $p_0$  is the initial pressure,  $\Gamma$  is the Gruneisen parameter,  $F_0$  is the initial fluence,  $\mu_0$  is a constant, and  $z$  is the depth of the tissue.<sup>96</sup> PAIs are reconstructed using a range of beamforming methodologies, akin to ultrasound imaging.<sup>94,96</sup> 3D tomographic images can be reconstructed by combining the temporal and spatial information collected, which is often achieved analytically using a simple back-projection inversion or numerically using model-based methods.<sup>96</sup> Images reconstructed from data acquired at several wavelengths can then be subjected to the same multivariate analysis methods described in Sec. 4 for spectral unmixing. However, frame-to-frame coregistration may be needed to avoid spatial or spectral corruption due to motion.

#### 5.1.4 Limitations

The attainable depth of PAI depends on the optical and acoustic attenuation of the sample. In soft tissue, acoustic attenuation scales as a function of ultrasound frequency, so at low frequencies of

a few MHz, optical attenuation tends to dominate and is the constraining factor for imaging depth.<sup>96</sup> For spatial resolution, the constraining factor is the bandwidth of the acoustic wave, usually limited by the acoustic attenuation of soft tissue and the frequency response of the detecting transducer.<sup>97</sup> The latter is particularly important for imaging more superficial features when the bandwidth of the signal can extend to 100 MHz and beyond, for which there is a limited availability of high-performance transducers. The maximum acoustic frequency transmitted decreases with depth, meaning that typically systems that operate at higher penetration depths have lower spatial resolutions than those designed for shallow imaging.<sup>97</sup>

A key challenge for PAI is biomarker quantification. During reconstruction, a number of assumptions are made; these include the speed of sound in tissue, transducer impulse response, detection bandwidth, and continuous sampling.<sup>96</sup> If these assumptions break down, for example, due to heterogeneities in tissue due to air cavities, there will be distortions in the image. Furthermore, when evaluating biomarkers such as THb and sO<sub>2</sub> the nature of light propagation in tissue can lead to distortions in the spectral properties of the illumination as a function of depth. Although some methods have been explored to compensate for such “spectral coloring,”<sup>94,222</sup> they often break down in the complex scenarios found in human tissue and have yet to be validated in a clinical setting. Finally, as with all hemoglobin sensing and imaging methods, calibration of the extracted biomarkers is vital. PAI calibration and clinical quality assurance methods are still under development, particularly through a community-led effort.<sup>98</sup>

## 5.2 Diffuse Optical Spectroscopy and Imaging

### 5.2.1 Clinical research studies

Diffuse optical spectroscopy (DOS) is commonly referred to as near-infrared spectroscopy (NIRS) because it uses light in the near-infrared range; the term functional NIRS (fNIRS) is also commonly used but is usually restricted to applications monitoring functional responses to stimuli in the brain via neurovascular coupling. Quantifying and monitoring changes in oxygenation of blood in the brain has found many applications that range from understanding seizures<sup>223</sup> to detecting brain damage.<sup>7</sup> Unlike reflectance hemoglobin imaging [Figs. 6(a)–6(d)], in which an open cranium is required (see Sec. 4), fNIRS typically achieves imaging depths of up to 15 mm through the skull [Figs. 6(e) and 6(f)], which covers the outer cerebral cortex in healthy adults.<sup>127,223–225</sup> fNIRS imaging of the brain to identify intracranial hematomas due to brain trauma has been clinically approved by the FDA recently; however, it has yet to be widely deployed in clinical settings.<sup>7</sup>

Similar to PAI, DOI has also been deployed in clinical trials to detect cancer, particularly in the breast<sup>226,227</sup> [Figs. 5(b) and 5(c)] and thyroid,<sup>127</sup> where it has also been used to monitor response to therapy. DOI tends to be lower in spatial resolution than PAI (Fig. 5), but it can often resolve other biomarkers in addition to hemoglobin. PAI typically has a lower temporal resolution compared with DOI.<sup>228,229</sup> In addition, DOI has been used to image muscle tissue such as the forearm, peripheral tissue, and joints.<sup>127,225</sup> Several reviews have been published illustrating the importance of DOI.<sup>230–233</sup>

### 5.2.2 Technology

DOI techniques typically use near-infrared light in the 650 to 900 nm range.<sup>127,225,228,230</sup> Below 650 nm, light can experience poor penetration due to the absorption of hemoglobin in superficial tissues, whereas above 920 nm, water absorption comes to dominate.<sup>225</sup> Most DOI and fNIRS systems use two (or more) different wavelengths, one that is in the lower range below the NIR isosbestic point, such as 680, 695, 705, or 730 nm, and another that has a longer wavelength, such as 830 or 850 nm. The number of light sources and detectors varies depending on the system from 1 to >48, with some designed to allow for more light sources and detectors to enable customization of spatial resolution according to the target application.<sup>228,234</sup>

DOS is similar to DOI but provides single-point measurements of tissue properties such as hemoglobin and blood oxygen saturation similar to pulse oximetry.<sup>235</sup> There are three main modalities of DOS/I: continuous wave (CW), time-domain (TD), and frequency-domain

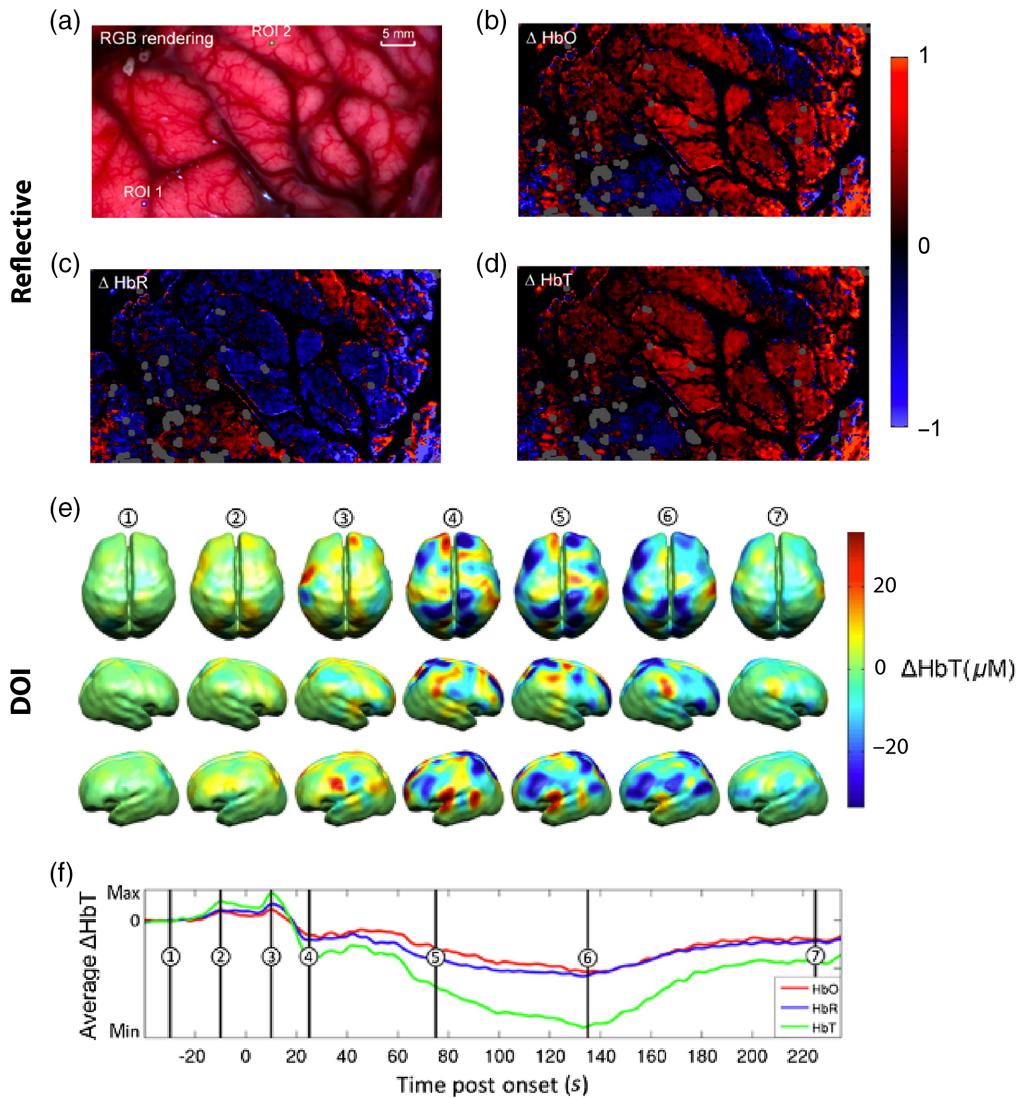


**Fig. 6** Hemoglobin imaging of the human brain. (a)–(d) Reflectance spectral images of the brain in an adult undergoing epileptogenic tissue resection (a) reference RGB rendering, (b) change in oxygenated hemoglobin over a single timeframe, (c) change in deoxygenated hemoglobin over a single timeframe, and (d) change in total hemoglobin over a single timeframe. Reproduced with permission from Ref. 76. (e), (f) DOI of a neonate during a seizure: (e) changes in HbT concentration mapped throughout the onset of a seizure and (f) average changes in Hb, HbO<sub>2</sub>, and tHb postonset of the seizure. Reproduced with permission from Ref. 223.

(FD) systems.<sup>127,225,228</sup> CW systems detect changes in the intensity of illumination, making them relatively simple and inexpensive.<sup>236</sup> Slight changes in surface coupling can affect the intensity measurements, resulting in poor reproducibility unless well controlled. TD systems correlate the time between emission and detection of photons to measure the photon flight time. Tissue scattering determines photon flight time, whereas absorption determines the overall intensity of photons reaching the detector. FD systems are based on similar principles to TD systems but instead measure the phase shift of the incoming light. Frequency domain systems are significantly less expensive than TD systems due to lower costs for the sensors and detectors. TD and FD systems can distinguish contaminating signals due to background illumination because these signals will be uncorrelated. Because TD and FD systems can separate out the effects of scattering and absorption, these techniques can quantify absolute concentrations of hemoglobin and its oxygenation, whereas CW systems typically measure the relative change in concentration but not the absolute quantities.

DOI can be deployed in different geometries, either topographic, with imaging of a single plane with limited depth information, or tomographic (DOT), including depth resolution, which allows for full 3D reconstruction of the pertinent properties of tissue. In transillumination techniques, the illumination and detection are on opposite sides of the tissue being imaged; however, this is limited to body parts with small radii. Measurements at multiple and overlapping source–detector separations can be used to create depth measurements and reconstruct a 3D image. In tomographic systems, the illumination and detection sensors are placed on the available surface to simultaneously measure the changes in illumination throughout the sample.

Finally, it is worth noting that diffuse correlation spectroscopy (DCS) is similar to DOI and DOS, but it uses an autocorrelation function through a combination of hardware and software to measure an index of blood flow in tissue [Fig. 5(c)].<sup>128</sup> Due to the similarities in apparatus, sometimes DCS is combined with DOI or DOS systems<sup>128</sup> to provide a spatially-resolved indication of blood flow as a complementary biomarker to THb or sO<sub>2</sub>.<sup>128</sup> Blood flow in tissue can also be detected using laser speckle contrast imaging (LCSI), which looks at fluctuations in the speckle pattern reflected from tissue to determine the flow rate of the blood.<sup>237,238</sup> Laser Doppler flowmetry (LDF) finds the flow rate and concentration of blood by quantifying the Doppler shift that causes spectral broadening of reflected light.<sup>238,239</sup> All three of these techniques can resolve flow rate, but they typically have relatively low spatial resolutions or are confined to single-point measurements. Recent advances, particularly in LCSI, are now reaching near real-time operation at higher spatial resolutions, benefitting from increased computing power available in portable systems.<sup>240</sup>

### 5.2.3 Analysis

The analysis for DOI depends on the type of imaging system used. The measured signals can be converted into optical absorption maps by understanding the transport of light in tissue, which can be modeled using the radiative transport equation (RTE)<sup>127,225</sup> or Monte Carlo methods. The RTE is an analytical approach that approximates Maxwell's equations in diffuse media, assuming a constant refractive index. Solving the RTE is computationally expensive,<sup>225</sup> but it can be sped up by exploiting symmetries or by making approximations. For example, the diffusion approximation assumes isotropic scattering,<sup>127</sup> so it can be applied only in diffusive tissues; it does not work well in nondiffusive tissue, such as the cerebrospinal fluid that surrounds the brain or in anisotropic media, such as the skin and nervous system, where prior information is required to reach a solution. Numerical techniques, such as the finite element method, finite difference method, finite volume method, and boundary element method, can be used to solve the diffusion approximation. The use of prior information such as MRI, CT, or other imaging techniques can vastly improve DOI resolution by reducing the number of assumptions about the tissue structure that are made.<sup>225</sup>

Light transport can also be understood by forward modeling the propagation of light using Monte Carlo methods to calculate the propagation of photons through media. The accumulated forward modeling statistics can then be analyzed with respect to real data from DOI systems to address the inverse scattering problem for various anisotropic scattering media.<sup>225</sup> Monte Carlo methods have traditionally also been computationally expensive, but they are now reaching higher speeds with deployment on GPU and cloud-based servers.<sup>241</sup>

### 5.2.4 Limitations

DOI exploits the scattering properties of tissue, unlike other imaging techniques that are hampered by light scattering. Despite this, DOI still has limited spatial resolution (on the order of 1 mm<sup>230</sup>) and often requires anatomical priors from another modality such as MRI or CT for analysis, which constrains applications<sup>127,225,230,235</sup> and adds cost and complexity to high-resolution DOI systems.<sup>225</sup> Standardization of DOI systems for clinical translation is ongoing, e.g., through a project to characterize DOI systems using phantoms,<sup>242</sup> particularly for breast cancer detection.<sup>243</sup>

### 5.3 Spectroscopic OCT

#### 5.3.1 Clinical research studies

While OCT is primarily deployed for structural imaging, its spectrally-resolved detection can be harnessed for angiography and oximetry *in vivo*, albeit not yet in clinical practice. OCT is typically implemented in the NIR for structural assessment due to its greater penetration through tissue and availability of light sources with suitable coherence. Extraction of blood  $sO_2$  from OCT measurements in human retinal vasculature was first demonstrated in the NIR (800/850 nm),<sup>244</sup> but it had limited precision due to weak absorption in this range. The development of visible OCT systems improved the available signal-to-noise ratio and hence precision, enabling measurements from single erythrocytes<sup>110,111</sup> and high-resolution capillary oximetry in 3D.<sup>112,113,245</sup> Advances in reconstruction algorithms and high-speed instrumentation have improved OCT angiography to a point at which it has found clinical use for high contrast imaging of retinal and dermal vasculature.<sup>246,247</sup> Visible OCT measurement of retinal  $sO_2$  has been tested in humans<sup>114</sup> alongside angiography,<sup>115</sup> but it is still in development. Laser exposure limits and natural aversion restrict the usable power level for visible OCT in the eye compared with clinical NIR OCT, but continuing improvements in OCT technology have allowed for high-quality imaging and  $sO_2$  measurement.

#### 5.3.2 Technology

OCT is a noncontact imaging modality that can be considered an optical analog of ultrasound imaging.<sup>116</sup> The distinguishing feature of OCT is the use of low-coherence interferometry to decouple the lateral and axial imaging resolution: lateral resolution is determined by the numerical aperture of the focusing optic, whereas axial resolution is determined by the temporal coherence of the laser used for imaging. Scanning OCT systems operate in the Fourier domain,<sup>248</sup> where a broad spectrum of light interrogates the tissue and is then collected through spectrally-resolved detection for postprocessing and image reconstruction by an inverse Fourier transform. Within this class, there are two major varieties: spectral-domain OCT (SD-OCT), which uses broadband illumination and parallel detection with a spectrometer, and swept-source OCT (SS-OCT), which uses a high-speed spectral scanning source with single-channel detection for temporally-resolved spectral acquisition.

Recent advances in SS-OCT laser technology, including the tunable vertical-cavity source emitting laser, have enabled the realization of high-speed, robust, and compact instruments, which leads to greater imaging depths. Current SS-OCT systems operate exclusively in the NIR range due to swept laser availability; for imaging performance (and potential Hb oximetry) in the visible domain, SD-OCT systems using a visible spectrometer are required. In recent years, the high power and spatial coherence of newly available supercontinuum lasers have enabled good-quality visible OCT imaging in research systems,<sup>117,249,250</sup> which could enable future developments toward clinical translation.

#### 5.3.3 Analysis

The raw data for SD-OCT are acquired from a high-speed spectrometer with line readout synchronized to a scanning mechanism, allowing for the mapping of each spectrum to a spatial position. The spectrum is normalized, filtered, and converted to a spatial reflectance profile, known as an A-line, through an inverse Fourier transform. For oximetry, the SD of this analysis must be narrowed, typically through a windowing function; although full spectral resolution of the OCT volume may be realized through the application of the short-time Fourier transform, the dependence of axial resolution on spectral bandwidth poses a necessary trade-off between spectral resolution and axial resolution in the spectroscopic OCT image. For  $sO_2$  measurement and spectral-contrast angiography, spectral windows are chosen to maximize the contrast of hemoglobin, typically in the range of 550 to 650 nm.<sup>112,251</sup> The spectrally-resolved total extinction coefficient is measured through depth fitting of the spectroscopic OCT A-line signal to the

Beer–Lambert law, from which the relative contributions of Hb and HbO<sub>2</sub> can be unmixed to determine sO<sub>2</sub>.

### 5.3.4 Limitations

OCT is highly versatile, being deployed for imaging the inner walls of blood vessels and luminal organs,<sup>252–256</sup> having an ultrawide field of view for scanning skin,<sup>257–259</sup> and with corrective lenses, compensating for ocular refraction in the ophthalmologic clinic. Nonetheless, there are several fundamental issues that are limiting its general adoption. First, the scanned acquisition adds instrumental complexity and can produce motion artifacts in patients. Although this is addressed in full-field OCT systems, these typically do not work with rough samples. Next, the spectral resolution of OCT imaging determines the maximum depth range that can be imaged, an aspect referred to as the sensitivity roll-off. Finally, because OCT is primarily sensitive to singly-scattered photons in tissue, the penetration depth of imaging is restricted to 1 to 2 mm in most human tissues. For this reason, large-scale clinical deployment of OCT has largely been limited to ophthalmology, dermatology, and cardiology, but creative advances in OCT probe and capsule technology will allow for continued *in situ* exploration of hemoglobin-related biomarkers from OCT in disease pathology throughout the body.<sup>256,260–262</sup>

## 6 Summary and Perspective

Moving beyond pulse oximetry to exploit the optical absorption of hemoglobin in imaging applications has shown significant promise in the clinic, with both superficial 2D and depth-resolved 3D implementations described in this review. Two wavelength THb and sO<sub>2</sub> imaging are already widely used in endoscopic and ophthalmic applications, respectively, and have reached large-scale clinical trials in depth-resolved PAI. Conversely, reflectance-based spectral imaging remains largely exploratory.

### 6.1 Trade Offs

Choosing the optimal hemoglobin imaging technique for a particular application involves consideration of several factors that often require trade-offs, including signal-to-noise ratio, spatial and temporal resolutions, target depth, and route to integration with existing clinical practice. Optical imaging techniques are ultimately restricted by the maximum permissible exposure at the illumination site, which places a fundamental limit on the signal-to-noise ratio available in the clinical setting. Some techniques are further restricted in the type of illumination used such as OCT, which requires coherent light, and PAI, which requires short, pulsed light; this can add to the complexity of safety considerations in the clinic.

Considering the factors of resolution and depth, reflectance-based imaging can achieve high spatiotemporal resolution in applications in which depth resolution is not vital, for example, with retinal, endoscopic, or intraoperative imaging. One could argue that depth-resolution will become increasingly prevalent with the emergence of more advanced solutions from spectroscopic OCT, PAI, and DOI, particularly as costs decrease. Nonetheless, depth-resolution typically implies a sacrifice of spatial or temporal resolution, which must be determined early in the discovery and development phase of the associated device. Furthermore, different approaches to achieving depth resolution have different strengths and weaknesses. PAI may suffer from shielding effects due to the absorption of overlying tissue and tends to resolve only larger vessels, whereas the use of multiple scattering by DOI enables better detection of capillary oxygenation, despite the overall poorer spatial resolution. This trade-off may explain why PAI has developed more rapidly in clinical translation for breast cancer detection, whereas DOI is more developed for imaging the brain. Given the common contrast source across many of the techniques described, it may also be desirable to combine multiple approaches in a single device for validation purposes or to provide views of the same tissue at different resolution scales, overcoming some of the limitations of the existing technologies.<sup>263</sup> Combining two or more optical imaging techniques can be beneficial because they reduce the imaging limitations that arise as

a result of a single technique. A good example of this is the enhanced perfusion oximetry system that combines diffuse reflectance spectroscopy with LDF to quantify blood oxygenation and flow rate for imaging of microvasculature and burns.<sup>264–266</sup>

## 6.2 Clinical Implementation

There are many factors to consider regarding the route to integration of new techniques into clinical practice. For example, if imaging is required to be non-contact, for example, in delicate targets like the eye, this may restrict the implementation of methods such as PAI or DOI, in which contact with the tissue is typically required. The pathway to clinical adoption may be smoother in the case of an existing optical imaging solution already being deployed. An obvious example is the large-scale deployment of OCT for ophthalmic applications, which provides a direct route for adoption of spectroscopic OCT in the community. Another factor in clinical translation is the assessment of the precision, accuracy, and bias of new biomarker measurements.<sup>2</sup> These factors can be affected by both device operation and data interpretation, requiring standardization of data acquisition and careful consideration of any signal processing or analysis methods applied before presenting the data to the interpreter, whether this is a human or a machine. Because reflectance-based imaging techniques are usually less computationally intensive compared with the depth-resolved methods, the development of systems and software for real-time imaging is more easily attainable; this is seen most effectively in narrowband imaging of blood vessels in endoscopy.

Further clinical considerations arise later in the translational pathway when the question of biomarker efficacy in decision-making finally arises. Instrument prototypes are often used first in pilot clinical trials at a single clinical center to gather initial data for validation and may be subject to multiple design iterations at this stage. Having successfully passed the first translational gap, which may include CE marking or FDA approval for the device and multicenter clinical trials, the technique is then subject to advanced qualification and ongoing technical validation to determine clinical utility in the healthcare setting, whereby the measurement can be used in clinical decision making. These larger-scale clinical trials help to determine sources of variation that will influence the classification and diagnosis of disease, providing clinical evidence of the ability to change patient management. They also provide extensive reference data sets that can be used to improve interpretation, particularly when machine learning-based methods are involved.

Reflectance-based spectral imaging techniques are still largely in the earlier stages of development with first in-person trials, whereas fNIRS of the brain and PAI of the breast are being used in multiple centers as part of larger-scale clinical trials and DOI has found some level of adoption into the clinic.<sup>71,87,208,228,231,267</sup> Data arising from these trials is extremely valuable and making annotated datasets open source for the community in the future will not only help accelerate the development of new algorithms but could also enhance our understanding of the biology of hemoglobin oxygenation in disease.

## 6.3 Disease Monitoring

Hemoglobin imaging methods could find further applications in monitoring disease, to detect treatment efficacy or disease relapse. The noninvasive nature of these techniques can allow for continuous or periodic monitoring, for which there are several excellent examples that have been highlighted. Pulse oximetry can be applied to a patient for long periods so that clinicians can observe if there are any changes to overall arterial oxygenation. DOI and NIRS also can be used longitudinally to monitor changes in brain function to assess if there is improved brain activity.<sup>267</sup> Furthermore, periodic monitoring of diseases such as scleroderma using nailfold capillaroscopy can indicate progression in the stage and severity of the disease, which may influence the treatment provided or indicate if further medical intervention is required.

Periodic monitoring can be applied in the short term, for monitoring wound or burn healing, or in the longer term in the context of endoscopic cancer surveillance in at-risk patient groups such as those with Barrett's esophagus that are at increased risk of developing cancer. The frequency of monitoring applied is determined by the disease being observed and the rate at which

change is expected, as well as by the training required for instrument use and data interpretation. For example, applying pulse oximetry is relatively quick with nonspecialists able to do it, and some more straightforward versions of capillaroscopy can be done using handheld devices. Conversely, endoscopies, OCT, DOI, and NIRS typically require training of specialist operators; hence it can be more expensive to conduct the procedures, meaning they are typically used for less frequent monitoring.

## 6.4 Outlook

The acceptability and relevance of new hemoglobin sensing and imaging technologies to clinicians will be driven by various factors, including cost, complexity, and physical size of the systems, as well as the ease of use and data interpretation. The commonplace use of pulse oximetry means that the clinical community is already well aware of the use of systemic sO<sub>2</sub> as a disease biomarker. Ongoing technological developments that lead to miniaturization of light sources, optical components, and cameras, as well as decreasing their cost, mitigate some of the technical limitations highlighted in this review. Advances in image processing, including convolutional neural networks, promise to aid in distilling rich datasets to actionable clinical information, enabling imaging systems to be more easily integrated into clinical care. Research questions remain regarding the sensitivity of hemoglobin sensing techniques in diverse populations and the diagnostic power of hemoglobin-derived biomarkers in the wide array of disease presentations included in this review, which will only be answered through comprehensive clinical trials. Hemoglobin imaging techniques add a new dimension of knowledge in a range of clinical settings, from capillaroscopy and endoscopy to intraoperative imaging; emerging technologies are well placed to further enhance these areas of existing clinical practice, but are also likely to contribute to the decentralization of healthcare to tertiary care centers and through the deployment of wearable technologies for self-monitoring in the home.

## Disclosure

The authors have no conflicts of interest to declare.

## Acknowledgments

M. T-W. acknowledges the financial support of the General Sir John Monash Foundation and the Cambridge Trust. GB was supported by the Gianna Angelopoulos Programme for Science Technology and Innovation. GS and SEB received funding from the EPSRC (EP/R003599/1) and CRUK (C9545/A29580).

## References

1. J. P. B. O'Connor et al., "Imaging biomarker roadmap for cancer studies," *Nat. Rev. Clin. Oncol.* **14**(3), 169–186 (2017).
2. D. J. Waterhouse et al., "A roadmap for the clinical implementation of optical-imaging biomarkers," *Nat. Biomed. Eng.* **3**(5), 339–353 (2019).
3. J. Levy et al., "Digital oximetry biomarkers for assessing respiratory function: standards of measurement, physiological interpretation, and clinical use," *NPJ Digit. Med.* **4**(1) (2021).
4. A. S. Scott, M. A. Baltzan, and N. Wolkove, "Examination of pulse oximetry tracings to detect obstructive sleep apnea in patients with advanced chronic obstructive pulmonary disease," *Can. Respir. J.* **21**(3), 171–175 (2014).
5. G. Dinsdale et al., "State-of-the-art technologies provide new insights linking skin and blood vessel abnormalities in SSc-related disorders," *Microvasc. Res.* **130**(April), 104006 (2020).
6. A. Nouvong et al., "Evaluation of diabetic foot ulcer healing with hyperspectral imaging of oxyhemoglobin and deoxyhemoglobin," *Diabetes Care* **32**(11), 2056–2061 (2009).

7. C. S. Robertson et al., "Clinical evaluation of a portable near-infrared device for detection of traumatic intracranial hematomas," *J. Neurotrauma* **27**(9), 1597–1604 (2010).
8. M. S. Chin et al., "Hyperspectral imaging for burn depth assessment in an animal model," *Plast. Reconstr. Surg. - Glob. Open* **3**(12), e591–9 (2015).
9. A. Roggan et al., "Optical properties of circulating human blood in the wavelength range 400–2500 nm," *J. Biomed. Opt.* **4**(1), 36–46 (1999).
10. M. L. Turgeon, *Clinical Hematology: Theory and Procedures*, 2nd ed., Little, Brown, Boston; London (1993).
11. I. J. Bigio and S. Fantini, "Overview of tissue optical properties," in *Quantitative Biomedical Optics: Theory, Methods, and Applications*, 1st ed., pp. 19–59, Cambridge University Press (2016).
12. T. Vos et al., "Global, regional, and national incidence, prevalence, and years lived with disability for 310 diseases and injuries, 1990–2015: a systematic analysis for the Global Burden of Disease Study 2015," *Lancet* **388**(10053), 1545–1602 (2016).
13. M. Nitzan, A. Romem, and R. Koppel, "Pulse oximetry: fundamentals and technology update," *Med. Devices Evid. Res.* **7**(1), 231–239 (2014).
14. W. Shin, Y. D. Cha, and G. Yoon, "ECG/PPG integer signal processing for a ubiquitous health monitoring system," *J. Med. Syst.* **34**(5), 891–898 (2010).
15. B. A. Darlow and C. J. Morley, "Oxygen saturation targeting and bronchopulmonary dysplasia," *Clin. Perinatol.* **42**(4), 807–823 (2015).
16. N. W. Tietz and E. A. Fiereck, "The spectrophotometric measurement of carboxyhemoglobin," *Ann. Clin. Lab. Sci.* **3**(1), 1388–1393 (1973).
17. L. Gharahbaghian, B. Massoudian, and G. Dimassa, "Methemoglobinemia and sulfhemoglobinemia in two pediatric patients after ingestion of hydroxylamine sulfate," *West. J. Emerg. Med.* **10**(3), 197–201 (2009).
18. E. Dervieux, Q. Bodinier, and W. Uhring, "Measuring hemoglobin spectra: searching for carbamino-hemoglobin," *J. Biomed. Opt.* **25**(10), 105001 (2020).
19. M. Van Gastel, S. Stuijk, and G. De Haan, "Camera-based pulse-oximetry - validated risks and opportunities from theoretical analysis," *Biomed. Opt. Express* **9**(1), 102 (2018).
20. J. K. Barton et al., "Cooperative phenomena in two-pulse, two-color laser photocoagulation of cutaneous blood vessels," *Photochem. Photobiol.* **73**(6), 642 (2001).
21. L. L. Randeberg et al., "Methemoglobin formation during laser induced photothermolysis of vascular skin lesions," *Lasers Surg. Med.* **34**(5), 414–419 (2004).
22. S. R. David et al., "The blood blues: a review on methemoglobinemia," *J. Pharmacol. Pharmacother.* **9**(1), 1–5 (2018).
23. C. S. Thom et al., "Hemoglobin variants: biochemical properties and clinical correlates," *Cold Spring Harb. Perspect. Med.* **3**(3), a011858 (2013).
24. L. Tofani et al., "Spectroscopic and interfacial properties of myoglobin/surfactant complexes," *Biophys. J.* **87**(2), 1186–1195 (2004).
25. L. S. L. Arakaki, D. H. Burns, and M. J. Kushmerick, "Accurate myoglobin oxygen saturation by optical spectroscopy measured in blood-perfused rat muscle," *Appl. Spectrosc.* **61**(9), 978–985 (2007).
26. G. Lu and B. Fei, "Medical hyperspectral imaging: a review," *J. Biomed. Opt.* **19**(1), 010901 (2014).
27. V. Tuchin, *Tissue Optics: Light Scattering Methods and Instruments for Medical Diagnosis*, 3rd ed., SPIE Press, Bellingham, Washington, USA (2015).
28. S. A. Prahl, "Tabulated molar extinction coefficient for hemoglobin in water," (1998). <http://omlc.org.edu/spectra/hemoglobin/summary.html>.
29. O. Siggaard-Andersen, B. Nørgaard-Pedersen, and J. Rem, "Hemoglobin pigments spectrophotometric determination of oxy-, carboxy-, met-, and sulfhemoglobin in capillary blood," *Clin. Chim. Acta* **42**(1), 85–100 (1972).
30. L. L. Randeberg and J. Hernandez-Palacios, "Hyperspectral imaging of bruises in the SWIR spectral region," *Proc. SPIE* **8207**, 82070N (2012).
31. I. H. Yarynovska and A. I. Bilyi, "Absorption spectra of sulfhemoglobin derivatives of human blood," *Proc. SPIE* **6094**, 60940G (2006).

32. J. Yao and L. V. Wang, "Sensitivity of photoacoustic microscopy," *Photoacoustics* **2**(2), 87–101 (2014).
33. W. G. Zijlstra, A. Buursma, and W. P. Meeuwse-van der Roest, "Absorption spectra of human fetal and adult oxyhemoglobin, de-oxyhemoglobin, carboxyhemoglobin, and methemoglobin," *Clin. Chem.* **37**(9), 1633–1638 (1991).
34. A. P. Harris et al., "Absorption characteristics of human fetal hemoglobin at wavelengths used in pulse oximetry," *J. Clin. Monit.* **4**(3), 175–177 (1988).
35. K. A. Shapovalov, "The geometry and optical models of the erythrocyte," *Syst. Rev. Pharm.* **11**(12), 1456–1463 (2020).
36. M. Kinnunen et al., "Effect of the size and shape of a red blood cell on elastic light scattering properties at the single-cell level," *Biomed. Opt. Express* **2**(7), 1803 (2011).
37. J. Gienger et al., "Refractive index of human red blood cells between 290 nm and 1100 nm determined by optical extinction measurements," *Sci. Rep.* **9**, 4623 (2019).
38. D. J. Faber, F. J. Van Der Meer, and M. C. G. Aalders, "Quantitative measurement of attenuation coefficients of weakly scattering media using optical coherence tomography," *Opt. Express* **12**(19), 4353–592 (2004).
39. R. Liu et al., "Theoretical model for optical oximetry at the capillary level: exploring hemoglobin oxygen saturation through backscattering of single red blood cells," *J. Biomed. Opt.* **22**(2), 025002 (2017).
40. R. Liu et al., "Single capillary oximetry and tissue ultrastructural sensing by dual-band dual-scan inverse spectroscopic optical coherence tomography," *Light Sci. Appl.* **7**(1), 57 (2018).
41. N. Bosschaart et al., "A literature review and novel theoretical approach on the optical properties of whole blood," *Lasers Med. Sci.* **29**(2), 453–479 (2014).
42. M. Meinke et al., "Optical properties of platelets and blood plasma and their influence on the optical behavior of whole blood in the visible to near infrared wavelength range," *J. Biomed. Opt.* **12**(1), 014024 (2007).
43. M. Meinke et al., "Empirical model functions to calculate hematocrit-dependent optical properties of human blood," *Appl. Opt.* **46**(10), 1742–1753 (2007).
44. M. Friebel et al., "Influence of oxygen saturation on the optical scattering properties of human red blood cells in the spectral range 250 to 2000 nm," *J. Biomed. Opt.* **14**(3), 034001 (2009).
45. T. Saito and H. Yamaguchi, "Optical imaging of hemoglobin oxygen saturation using a small number of spectral images for endoscopic imaging," *J. Biomed. Opt.* **20**(12), 126011 (2015).
46. S. L. Jacques, "Optical properties of biological tissues: a review," *Phys. Med. Biol.* **58**(11), R37–R61 (2013).
47. A. J. Welch, M. J. C. van Gemert, and J. T. Walsh, "Basic Interactions of Light with Tissue," in *Optical-Thermal Response of Laser-Irradiated Tissue*, pp. 13–26, Springer Netherlands, Dordrecht (2011).
48. A. Reisner et al., "Utility of the photoplethysmogram in circulatory monitoring," *Anesthesiology* **108**(5), 950–958 (2008).
49. J. E. Sinex, "Pulse oximetry: principles and limitations," *Am. J. Emerg. Med.* **17**(1), 59–66 (1999).
50. G. Tusman, S. H. Bohm, and F. Suarez-Sipmann, "Advanced uses of pulse oximetry for monitoring mechanically ventilated patients," *Anesth. Analg.* **124**(1), 62–71 (2017).
51. H. Lee et al., "Toward all-day wearable health monitoring: an ultralow-power, reflective organic pulse oximetry sensing patch," *Sci. Adv.* **4**(11), 1–9 (2018).
52. S. Lopez, *Pulse Oximeter Fundamentals and Design*, pp. 1–39, Free Semiconductor Inc. (2012).
53. O. Y. Hay et al., "Pulse oximetry with two infrared wavelengths without calibration in extracted arterial blood," *Sensors (Switzerland)* **18**(10), 3457 (2018).
54. M. P. McEwen, G. P. Bull, and K. J. Reynolds, "Vessel calibre and haemoglobin effects on pulse oximetry," *Physiol. Meas.* **30**(9), 869–883 (2009).
55. E. Hill and M. D. Stoneham, "Practical applications of pulse oximetry," *Updat. Anaesth.* **5**(11), 11–15 (2000).

56. T. Y. Abay and P. A. Kyriacou, "Comparison of NIRS, laser Doppler flowmetry, photoplethysmography, and pulse oximetry during vascular occlusion challenges," *Physiol. Meas.* **37**(4), 503–514 (2016).
57. C. Liu et al., "Optical fibre-based pulse oximetry sensor with contact force detection," *Sensors (Switzerland)* **18**(11), 3632 (2018).
58. W. Verkruyse et al., "Calibration of contactless pulse oximetry," *Anesth. Analg.* **124**(1), 136–145 (2017).
59. J. Kim et al., "Miniaturized battery-free wireless systems for wearable pulse oximetry," *Adv. Funct. Mater.* **27**(1), 1–8 (2017).
60. S. N. Lambova and U. Müller-Ladner, "Nailfold capillaroscopy in systemic sclerosis – state of the art: the evolving knowledge about capillaroscopic abnormalities in systemic sclerosis," *J. Scleroderma Relat. Disord.* **4**(3), 200–211 (2019).
61. M. V. Volkov et al., "Video capillaroscopy clarifies mechanism of the photoplethysmographic waveform appearance," *Sci. Rep.* **7**, 13298 (2017).
62. J. Aguirre et al., "Assessing nailfold microvascular structure with ultra-wideband raster-scan optoacoustic mesoscopy," *Photoacoustics* **10**, 31–37 (2018).
63. A. K. Murray et al., "Noninvasive imaging techniques in the assessment of scleroderma spectrum disorders," *Arthritis Care Res.* **61**(8), 1103–1111 (2009).
64. A. Karbalaie et al., "Practical issues in assessing nailfold capillaroscopic images: a summary," *Clin. Rheumatol.* **38**(9), 2343–2354 (2019).
65. D. Paxton and J. D. Pauling, "Does nailfold capillaroscopy help predict future outcomes in systemic sclerosis? A systematic literature review," *Semin. Arthritis Rheum.* **48**(3), 482–494 (2018).
66. M. Berks et al., "An automated system for detecting and measuring nailfold capillaries," *Lect. Notes Comput. Sci.* **8673**, 658–665 (2014).
67. M. E. Anderson et al., "Computerized nailfold video capillaroscopy - a new tool for assessment of Raynaud's phenomenon," *J. Rheumatol.* **32**(5), 841–848 (2005).
68. G. N. McKay, N. Mohan, and N. J. Durr, "Imaging human blood cells in vivo with oblique back-illumination capillaroscopy," *Biomed. Opt. Express* **11**(5), 2373 (2020).
69. M. Michalska-Jakubus et al., "Plasma endothelial microparticles reflect the extent of capillaroscopic alterations and correlate with the severity of skin involvement in systemic sclerosis," *Microvasc. Res.* **110**, 24–31 (2017).
70. B. Ruaro et al., "Correlations between skin blood perfusion values and nailfold capillaroscopy scores in systemic sclerosis patients," *Microvasc. Res.* **105**, 119–124 (2016).
71. N. T. Clancy et al., "Surgical spectral imaging," *Med. Image Anal.* **63**, 101699 (2020).
72. J. Yoon et al., "A clinically translatable hyperspectral endoscopy (HySE) system for imaging the gastrointestinal tract," *Nat. Commun.* **10**, 1902 (2019).
73. A. S. Luthman et al., "Bimodal reflectance and fluorescence multispectral endoscopy based on spectrally resolving detector arrays," *J. Biomed. Opt.* **24**(3), 031009 (2018).
74. R. Podlipiec et al., "Characterization of blood coagulation dynamics and oxygenation in ex-vivo retinal vessels by fluorescence hyperspectral imaging," *J. Biophotonics* **13**(8), 1–12 (2020).
75. X. Hadoux et al., "Non-invasive in vivo hyperspectral imaging of the retina for potential biomarker use in Alzheimer's disease," *Nat. Commun.* **10**, 49 (2019).
76. J. Pichette et al., "Intraoperative video-rate hemodynamic response assessment in human cortex using snapshot hyperspectral optical imaging," *Neurophotonics* **3**(4), 045003 (2016).
77. L. C. Cancio, "Application of novel hyperspectral imaging technologies in combat casualty care," *Proc. SPIE* **7596**, 759605 (2010).
78. A. S. Luthman, *Spectrally Resolved Detector Arrays for Multiplexed Biomedical Fluorescence Imaging*, Springer International Publishing, Cham (2018).
79. S. Grusche, "Basic slit spectroscopy reveals three-dimensional scenes through diagonal slices of hyperspectral cubes," *Appl. Opt.* **53**(20), 4594 (2014).
80. M. Ewerlöf, M. Larsson, and E. G. Sallerud, "Spatial and temporal skin blood volume and saturation estimation using a multispectral snapshot imaging camera," *Proc. SPIE* **10068**, 1006814 (2017).

81. N. Hagen and M. W. Kudenov, "Review of snapshot spectral imaging technologies," *Opt. Eng.* **52**(9), 090901 (2013).
82. M. Torabzadeh et al., "Hyperspectral imaging in the spatial frequency domain with a super-continuum source," *J. Biomed. Opt.* **24**(7), 071614 (2019).
83. M. A. Wares et al., "Noninvasive evaluation of hemodynamics and light scattering property during two-stage mouse cutaneous carcinogenesis based on multispectral diffuse reflectance images at isosbestic wavelengths of hemoglobin," *J. Biomed. Opt.* **24**(3), 031020 (2019).
84. D. J. Waterhouse et al., "Emerging optical methods for endoscopic surveillance of Barrett's oesophagus," *Lancet Gastroenterol. Hepatol.* **3**(5), 349–362 (2018).
85. T. Chiba et al., "Advanced multispectral image-processing endoscopy system for visualizing two-dimensional hemoglobin saturation and relative hemoglobin concentration," *Endosc. Int. Open* **7**(11), E1442–E1447 (2019).
86. L. Lin et al., "Single-breath-hold photoacoustic computed tomography of the breast," *Nat. Commun.* **9**, 2352 (2018).
87. M. Li, Y. Tang, and J. Yao, "Photoacoustic tomography of blood oxygenation: a mini review," *Photoacoustics* **10**, 65–73 (2018).
88. J. Jo et al., "A functional study of human inflammatory arthritis using photoacoustic imaging," *Sci. Rep.* **7**, 15026 (2017).
89. S. Manohar and M. Dantuma, "Current and future trends in photoacoustic breast imaging," *Photoacoustics* **16**, 100134 (2019).
90. P. K. Upputuri and M. Pramanik, "Recent advances toward preclinical and clinical translation of photoacoustic tomography: a review," *J. Biomed. Opt.* **22**(4), 041006 (2016).
91. W. C. Chapman and M. Mutch, "Co-registered photoacoustic and ultrasound imaging of human colorectal cancer," *J. Biomed. Opt.* **24**(12), 121913 (2019).
92. G. S. Sangha and C. J. Goergen, "Label-free photoacoustic and ultrasound imaging for murine atherosclerosis characterization," *APL Bioeng.* **4**(2), 026102 (2020).
93. Y. Wang et al., "A portable three-dimensional photoacoustic tomography system for imaging of chronic foot ulcers," *Quantum Imaging Med. Surg.* **9**(5), 799–799 (2019).
94. V. Ntziachristos and D. Razansky, "Molecular imaging by means of multispectral optoacoustic tomography (MSOT)," *Chem. Rev.* **110**(5), 2783–2794 (2010).
95. E. Maneas et al., "Photoacoustic imaging of the human placental vasculature," *J. Biophotonics* **13**(4), 1–10 (2020).
96. M. Xu and L. V. Wang, "Photoacoustic imaging in biomedicine," *Rev. Sci. Instrum.* **77**(4), 041101 (2006).
97. P. Beard, "Biomedical photoacoustic imaging," *Interface Focus* **1**(4), 602–631 (2011).
98. S. Bohndiek, "Addressing photoacoustics standards," *Nat. Photonics* **13**(5), 298 (2019).
99. G. Ku et al., "Multiple-bandwidth photoacoustic tomography," *Phys. Med. Biol.* **49**(7), 1329–1338 (2004).
100. T. P. Nguyen et al., "Improved depth-of-field photoacoustic microscopy with a multifocal point transducer for biomedical imaging," *Sensors (Switzerland)* **20**(7), 1–18 (2020).
101. C. Chu et al., "Multimodal photoacoustic imaging-guided regression of corneal neovascularization: a non-invasive and safe strategy," *Adv. Sci.* **2000346**, 1–7 (2020).
102. M. Martinho Costa et al., "Quantitative photoacoustic imaging study of tumours in vivo: baseline variations in quantitative measurements," *Photoacoustics* **13**, 53–65 (2019).
103. P. Zhang et al., "High-resolution deep functional imaging of the whole mouse brain by photoacoustic computed tomography in vivo," *J. Biophotonics* **11**(1), 1–6 (2018).
104. R. Haindl et al., "Functional optical coherence tomography and photoacoustic microscopy imaging for zebrafish larvae," *Biomed. Opt. Express* **11**(4), 2137 (2020).
105. H. Leng et al., "Characterization of a fiber bundle-based real-time ultrasound/photoacoustic imaging system and its in vivo functional imaging applications," *Micromachines* **10**(12), 820 (2019).
106. A. Hariri et al., "The characterization of an economic and portable LED-based photoacoustic imaging system to facilitate molecular imaging," *Photoacoustics* **9**, 10–20 (2018).
107. Y. Junjie et al., "High-speed label-free functional photoacoustic microscopy of mouse brain in action," *Nat. Methods* **12**(4), 407–410 (2015).

108. H. F. Zhang et al., “Functional photoacoustic microscopy for high-resolution and noninvasive in vivo imaging,” *Nat. Biotechnol.* **24**(7), 848–851 (2006).
109. A. Taruttis and V. Ntziachristos, “Advances in real-time multispectral optoacoustic imaging and its applications,” *Nat. Photonics* **9**(4), 219–227 (2015).
110. J. Yi and X. Li, “Estimation of oxygen saturation from erythrocytes by high-resolution spectroscopic optical coherence tomography,” *Opt. Lett.* **35**(12), 2094 (2010).
111. F. E. Robles, S. Chowdhury, and A. Wax, “Assessing hemoglobin concentration using spectroscopic optical coherence tomography for feasibility of tissue diagnostics,” *Biomed. Opt. Express* **1**(1), 310–317 (2010).
112. J. A. Winkelmann et al., “Spectral contrast optical coherence tomography angiography enables single-scan vessel imaging,” *Light Sci. Appl.* **8**(1), 7 (2019).
113. S. Pi et al., “Retinal capillary oximetry with visible light optical coherence tomography,” *Proc. Natl. Acad. Sci. U. S. A.* **117**(21), 11658–11666 (2020).
114. S. Chen et al., “Retinal oximetry in humans using visible-light optical coherence tomography [Invited],” *Biomed. Opt. Express* **8**(3), 1415 (2017).
115. W. Song et al., “Visible light optical coherence tomography angiography (vis-OCTA) facilitates local microvascular oximetry in the human retina,” *Biomed. Opt. Express* **11**(7), 4037 (2020).
116. D. Huang et al., “Optical coherence tomography,” *Science* **254**(5035), 1178–1181 (1991).
117. J. Yi et al., “Visible-light optical coherence tomography for retinal oximetry,” *Opt. Lett.* **38**(11), 1796–1798 (2013).
118. S. Chen et al., “Imaging hemodynamic response after ischemic stroke in mouse cortex using visible-light optical coherence tomography,” *Biomed. Opt. Express* **7**(9), 3377 (2016).
119. P. L. Nesper et al., “OCT angiography and visible-light OCT in diabetic retinopathy,” *Vision Res.* **139**, 191–203 (2017).
120. S. Pi et al., “Automated spectroscopic retinal oximetry with visible-light optical coherence tomography,” *Biomed. Opt. Express* **9**(5), 2056 (2018).
121. B. T. Soetikno et al., “Inner retinal oxygen metabolism in the 50/10 oxygen-induced retinopathy model,” *Sci. Rep.* **5**, 16752 (2015).
122. W. Liu et al., “Increased retinal oxygen metabolism precedes microvascular alterations in type 1 diabetic mice,” *Investig. Ophthalmol. Vis. Sci.* **58**(2), 981–989 (2017).
123. D. J. Cuccia et al., “Quantitation and mapping of tissue optical properties using modulated imaging,” *J. Biomed. Opt.* **14**(2), 024012 (2009).
124. N. C. Biswal, Y. Xu, and Q. Zhu, “Imaging tumor oxyhemoglobin and deoxyhemoglobin concentrations with ultrasound-guided diffuse optical tomography,” *Technol. Cancer Res. Treat.* **10**(5), 417–429 (2011).
125. D. Orive-Miguel et al., “Real-time dual-wavelength time-resolved diffuse optical tomography system for functional brain imaging based on probe-hosted silicon photomultipliers,” *Sensors (Switzerland)* **20**(10), 2815 (2020).
126. Y. Wang et al., “Combined diffuse optical tomography and photoacoustic tomography for enhanced functional imaging of small animals: a methodological study on phantoms,” *Appl. Opt.* **56**(2), 303 (2017).
127. Y. Hoshi and Y. Yamada, “Overview of diffuse optical tomography and its clinical applications,” *J. Biomed. Opt.* **21**(9), 091312 (2016).
128. Y. Shang, T. Li, and G. Yu, “Clinical applications of near-infrared diffuse correlation spectroscopy and tomography for tissue blood flow monitoring and imaging,” *Physiol. Meas.* **38**(4), R1–R26 (2017).
129. F. Picot et al., “Interstitial imaging with multiple diffusive reflectance spectroscopy projections for in vivo blood vessels detection during brain needle biopsy procedures,” *Neurophotonics* **6**(2), 025003 (2019).
130. V. C. Kavuri et al., “Sparsity enhanced spatial resolution and depth localization in diffuse optical tomography,” *Biomed. Opt. Express* **3**(5), 943–957 (2012).
131. R. Baikejiang, W. Zhang, and C. Li, “Diffuse optical tomography for breast cancer imaging guided by computed tomography: a feasibility study,” *J. Xray. Sci. Technol.* **25**(3), 341–355 (2017).

132. S. Brigadoi et al., "A 4D neonatal head model for diffuse optical imaging of pre-term to term infants," *Neuroimage* **100**, 385–394 (2014).
133. M. A. Khalil et al., "Dynamic diffuse optical tomography imaging of peripheral arterial disease," *Biomed. Opt. Express* **3**(9), 2288 (2012).
134. D. A. Boas et al., "Establishing the diffuse correlation spectroscopy signal relationship with blood flow," *Neurophotonics* **3**(3), 031412 (2016).
135. P. D. Mannheim, "The light-tissue interaction of pulse oximetry," *Anesth. Analg.* **105**(6), S10–S17 (2007).
136. J. T. B. Moyle, "Uses and abuses of pulse oximetry," *Arch. Dis. Child.* **74**(1), 77–80 (1996).
137. A. M. Luks and E. R. Swenson, "Pulse oximetry for monitoring patients with COVID-19 at home potential pitfalls and practical guidance," *Ann. Am. Thorac. Soc.* **17**(9), 1040–1046 (2020).
138. A. Jubran, "Pulse oximetry," *Intensive Care Med.* **31**(11), 1598 (2005).
139. M. Kluckow, "Barriers to the implementation of newborn pulse oximetry screening: a different perspective," *Int. J. Neonatal Screen.* **4**(1), 4 (2018).
140. Z. Mosayebi et al., "Evaluation of pulse oximetry in the early diagnosis of cardiac and noncardiac diseases in healthy newborns," *Iran. J. Neonatol.* **11**(1), 43–50 (2020).
141. A. Fawzy et al., "Racial and ethnic discrepancy in pulse oximetry and delayed identification of treatment eligibility among patients with COVID-19," *JAMA Intern Med.* **182**(7), 730–738 (2022).
142. M. W. Sjoding et al., "Racial bias in pulse oximetry measurement," *N. Engl. J. Med.* **383**(25), 2477–2478 (2020).
143. A. Jubran, "Pulse oximetry," *Intensive Care Med.* **19**(1), 1–7 (2005).
144. E. D. Chan, M. M. Chan, and M. M. Chan, "Pulse oximetry: understanding its basic principles facilitates appreciation of its limitations," *Respir. Med.* **107**(6), 789–799 (2013).
145. R. W. C. G. R. Wijshoff et al., "Reducing motion artifacts in photoplethysmograms by using relative sensor motion: phantom study," *J. Biomed. Opt.* **17**(11), 117007 (2012).
146. H. Zhang et al., "Wireless, battery-free optoelectronic systems as subdermal implants for local tissue oximetry," *Sci. Adv.* **5**(3) (2019).
147. J. Nixdorff et al., "Comparison of transmittance and reflectance pulse oximetry in anesthetized dogs," *Front. Vet. Sci.* **8**(April), 1–7 (2021).
148. L. E. Mackenzie and A. R. Harvey, "Oximetry using multispectral imaging: theory and application," *J. Opt. (United Kingdom)* **20**(6), 063501 (2018).
149. M. Nitzan and S. Engelberg, "Three-wavelength technique for the measurement of oxygen saturation in arterial blood and in venous blood," *J. Biomed. Opt.* **14**(2), 024046 (2009).
150. Q. J. W. Milner and G. R. Mathews, "An assessment of the accuracy of pulse oximeters," *Anaesthesia* **67**(4), 396–401 (2012).
151. M. Oura et al., "Calibration system for pulse spectrophotometry using a double-layer pulsation flow-cell," in *Proc. 31st Annu. Int. Conf. IEEE Eng. Med. Biol. Soc. Eng. Futur. Biomed. EMBC*, IEEE, pp. 896–899 (2009).
152. V. N. D. Le et al., "Calibration of spectral imaging devices with oxygenation-controlled phantoms: introducing a simple gel-based hemoglobin model," *Front. Phys.* **7**(November), 1–7 (2019).
153. J. E. Yount, "Devices and procedures for in vitro testing of pulse oximetry monitors," 4,968,137, p. US Patent: 4,968,137, United States (1990).
154. S. J. Barker and K. K. Tremper, "The effect of carbon monoxide inhalation on pulse oximetry and transcutaneous PO<sub>2</sub>," *Anesthesiology* **66**(5), 677–679 (1987).
155. Clinical Dynamics Corporation, "Smart Sat TM Pulse Oximetry Analyzer," pp. 1–42 (2004).
156. M. Nitzan et al., "Calibration-free pulse oximetry based on two wavelengths in the infrared - a preliminary study," *Sensors (Switzerland)* **14**(4), 7420–7434 (2014).
157. S. J. Barker et al., "Measurement of carboxyhemoglobin and methemoglobin by pulse oximetry: a human volunteer study," *Anesthesiology* **105**(5), 892–897 (2006).
158. P. E. Bicikler, J. R. Feiner, and J. W. Severinghaus, "Effects of skin pigmentation on pulse oximeter accuracy at low saturation," *Anesthesiology* **102**(4), 715–719 (2005).

159. Q. Li et al., “Review of spectral imaging technology in biomedical engineering: achievements and challenges,” *J. Biomed. Opt.* **18**(10), 100901 (2013).
160. P. Lukes et al., “Narrow band imaging (NBI) — endoscopic method for detection of head and neck cancer,” *Endoscopy* **5**, 75–87 (2013).
161. Q. Li et al., “Estimation of tissue oxygen saturation from RGB images and sparse hyperspectral signals based on conditional generative adversarial network,” *Int. J. Comput. Assist. Radiol. Surg.* **14**(6), 987–995 (2019).
162. D. S. Terman et al., “Sickle erythrocytes target cytotoxics to hypoxic tumor microvessels and potentiate a tumoricidal response,” *PLoS One* **8**(1), e52543 (2013).
163. H. L. Offerhaus, S. E. Bohndiek, and A. R. Harvey, “Hyperspectral imaging in biomedical applications,” *J. Opt. (United Kingdom)* **21**(1), 010202 (2019).
164. E. Häggblad et al., “Reflection spectroscopy of analgesized skin,” *Microvasc. Res.* **62**(3), 392–400 (2001).
165. L. Giannoni, F. Lange, and I. Tachtsidis, “Hyperspectral imaging solutions for brain tissue metabolic and hemodynamic monitoring: past, current and future developments,” *J. Opt. (United Kingdom)* **20**(4), 44009 (2018).
166. T. W. Sawyer et al., “Opti-MSFA: a toolbox for generalized design and optimization of multispectral filter arrays,” *Opt. Express* **30**(5), 7591 (2022).
167. M. Taylor-Williams et al., “Spectrally tailored ‘hyperpixel’ filter arrays for imaging of chemical compositions,” *Proc. SPIE* **11954**, 1195406 (2022).
168. S. Beg, A. Wilson, and K. Ragunath, “The use of optical imaging techniques in the gastrointestinal tract,” *Frontline Gastroenterol.* **7**(3), 207–215 (2016).
169. S. J. Spechler et al., “American gastroenterological association technical review on the management of Barrett’s esophagus,” *Gastroenterology* **140**(3), e18–e52 (2011).
170. J. Yoon et al., “First experience in clinical application of hyperspectral endoscopy for evaluation of colonic polyps,” *J. Biophotonics* **14**(9), 1–9 (2021).
171. D. J. Waterhouse et al., “Spectral endoscopy enhances contrast for neoplasia in surveillance of Barrett’s esophagus,” *Cancer Res.* **81**(12), 3415–3425 (2021).
172. V. Dremin et al., “Dynamic evaluation of blood flow microcirculation by combined use of the laser Doppler flowmetry and high-speed videocapillaroscopy methods,” *J. Biophotonics* **12**(6), 1–7 (2019).
173. M. V. Volkov et al., “Evaluation of blood microcirculation parameters by combined use of laser Doppler flowmetry and videocapillaroscopy methods,” *Proc. SPIE* **10336**, 1033607 (2017).
174. U. Baran, L. Shi, and R. K. Wang, “Capillary blood flow imaging within human finger cuticle using optical microangiography,” *J. Biophotonics* **8**(1–2), 46–51 (2015)..
175. W. F. Yip et al., “Reliability and determinants of retinal vessel oximetry measurements in healthy eyes,” *Invest. Ophthalmol. Vis. Sci.* **55**(11), 7104–7110 (2014).
176. A. K. Garg et al., “Advances in retinal oximetry,” *Transl. Vis. Sci. Technol.* **10**(2), 5–18 (2021).
177. J. M. Kainerstorfer et al., “Quantitative principal component model for skin chromophore mapping using multi-spectral images and spatial priors,” *Biomed. Opt. Express* **2**(5), 1040 (2011).
178. K. Kikuchi, Y. Masuda, and T. Hirao, “Imaging of hemoglobin oxygen saturation ratio in the face by spectral camera and its application to evaluate dark circles,” *Ski. Res. Technol.* **19**(4), 499–507 (2013).
179. Q. He and R. Wang, “Hyperspectral imaging enabled by an unmodified smartphone for analyzing skin morphological features and monitoring hemodynamics,” *Biomed. Opt. Express* **11**(2), 895 (2020).
180. E. Zherebtsov et al., “Hyperspectral imaging of human skin aided by artificial neural networks,” *Biomed. Opt. Express* **10**(7), 3545 (2019).
181. N. T. Clancy et al., “Intraoperative measurement of bowel oxygen saturation using a multi-spectral imaging laparoscope,” *Biomed. Opt. Express* **6**(10), 4179 (2015).
182. T. Pruijboom et al., “Perioperative hyperspectral imaging to assess mastectomy skin flap and DIEP flap perfusion in immediate autologous breast reconstruction: a pilot study,” *Diagnostics* **12**(1), 184 (2022).

183. J. M. Eichenholz et al., “Real-time megapixel multispectral bioimaging,” *Proc. SPIE* **7568**, 75681L (2010).
184. R. Calvini, A. Ulrici, and J. M. Amigo, “Growing applications of hyperspectral and multispectral imaging,” *Data Handl. Sci. Technol.* **32**, 605–629 (2020).
185. T. W. Sawyer, C. Williams, and S. E. Bohndiek, “Spectral band selection and tolerancing for multispectral filter arrays,” in *Front. Opt. - Proc. Front. Opt. + Laser Sci. APS/DLS*, pp. 3–5 (2019).
186. C. Williams et al., “Grayscale-to-color: scalable fabrication of custom multispectral filter arrays,” *ACS Photonics* **6**(12), 3132–3141 (2019).
187. R. Wu et al., “Optimized multi-spectral filter arrays for spectral reconstruction,” *Sensors (Switzerland)* **19**(13), 2905 (2019).
188. S. Gioux, A. Mazhar, and D. J. Cuccia, “Spatial frequency domain imaging in 2019: principles, applications, and perspectives,” *J. Biomed. Opt.* **24**(7), 071613 (2019).
189. R. H. Wilson et al., “High-speed spatial frequency domain imaging of rat cortex detects dynamic optical and physiological properties following cardiac arrest and resuscitation,” *Neurophotonics* **4**(4), 045008 (2017).
190. M. T. Ghijsen et al., “Quantitative real-time optical imaging of the tissue metabolic rate of oxygen consumption,” *J. Biomed. Opt.* **23**(3), 036013 (2018).
191. M. Schmidt et al., “Real-time, wide-field, and quantitative oxygenation imaging using spatiotemporal modulation of light,” *J. Biomed. Opt.* **24**(7), 071610 (2019).
192. C. Weinkauff et al., “Near-instant noninvasive optical imaging of tissue perfusion for vascular assessment,” *J. Vasc. Surg.* **69**(2), 555–562 (2019).
193. S. Jett et al., “Stratification of microvascular disease severity in the foot using spatial frequency domain imaging,” *J. Diabetes Sci. Technol.* 19322968211024666 (2021).
194. A. Ponticorvo et al., “Spatial frequency domain imaging (SFDI) of clinical burns: a case report,” *Burn. Open* **4**(2), 67–71 (2020).
195. J. Sun et al., “Enhancing in vivo tumor boundary delineation with structured illumination fluorescence molecular imaging and spatial gradient mapping,” *J. Biomed. Opt.* **21**(8), 080502 (2016).
196. D. Wirth et al., “Feasibility of using spatial frequency-domain imaging intraoperatively during tumor resection,” *J. Biomed. Opt.* **24**(7), 071608 (2018).
197. P. A. Valdes et al., “qF-SSOP: real-time optical property corrected fluorescence imaging,” *Biomed. Opt. Express* **8**(8), 3597 (2017).
198. Y. Garini, I. T. Young, and G. McNamara, “Spectral imaging: principles and applications,” *Cytom. Part A* **69**(8), 735–747 (2006).
199. J. Wei and X. Wang, “An overview on linear unmixing of hyperspectral data,” *Math. Probl. Eng.* **2020**, 3735403 (2020).
200. M. D. Mura, J. Chanussot, and A. Plaza, *An Overview on Hyperspectral Unmixing*, GIPSA-Lab, Grenoble Inst. Technology (2014).
201. J. S. Bhatt and M. V. Joshi, “Deep learning in hyperspectral unmixing: a review,” in *Int. Geosci. Remote Sens. Symp.*, pp. 2189–2192 (2020).
202. A. Grigoriou, J. Yoon, and S. E. Bohndiek, “Deep learning applied to hyperspectral endoscopy for online spectral classification,” *Sci. Rep.* **10**, 3947 (2020).
203. S. Li et al., “Deep learning for hyperspectral image classification: an overview,” *IEEE Trans. Geosci. Remote Sens.* **57**(9), 6690–6709 (2019).
204. J. Gröhl et al., “Learned spectral decoloring enables photoacoustic oximetry,” *Sci. Rep.* **11**, 6565 (2021).
205. S. Agrawal et al., “Functional, molecular and structural imaging using LED-based photoacoustic and ultrasound imaging system,” *Proc. SPIE* **11240**, 112405A (2020).
206. D. Lighter et al., “Multispectral, non-contact diffuse optical tomography of healthy human finger joints,” *Biomed. Opt. Express* **9**(4), 1445 (2018).
207. S. P. Chong et al., “Cerebral metabolic rate of oxygen (CMRO<sub>2</sub>) assessed by combined Doppler and spectroscopic OCT,” *Biomed. Opt. Express* **6**(10), 3941 (2015).
208. E. Brown, J. Bruncker, and S. E. Bohndiek, “Photoacoustic imaging as a tool to probe the tumour microenvironment,” *DMM Dis. Model. Mech.* **12**(7), dmm039636 (2019).
209. I. Steinberg et al., “Photoacoustic clinical imaging,” *Photoacoustics* **14**, 77–98 (2019).

210. T. Shiina, M. Toi, and T. Yagi, "Development and clinical translation of photoacoustic mammography," *Biomed. Eng. Lett.* **8**(2), 157–165 (2018).
211. P. G. Anderson et al., "Broadband optical mammography: chromophore concentration and hemoglobin saturation contrast in breast cancer," *PLoS One* **10**(3), 1–23 (2015).
212. L. He et al., "Noncontact diffuse correlation tomography of human breast tumor," *J. Biomed. Opt.* **20**(8), 086003 (2015).
213. E. I. Neuschler et al., "Breast imaging: optoacoustic imaging to diagnose benign and malignant breast masses Neuschler et al materials and methods," *Radiology* **287**(2) (2017).
214. M. Omar, J. Aguirre, and V. Ntziachristos, "Optoacoustic mesoscopy for biomedicine," *Nat. Biomed. Eng.* **3**(5), 354–370 (2019).
215. G. L. G. Menezes et al., "Downgrading of breast masses suspicious for cancer by using optoacoustic breast imaging," *Radiology* **288**(2), 355–365 (2018).
216. W. Roll et al., "Multispectral optoacoustic tomography of benign and malignant thyroid disorders: a pilot study," *J. Nucl. Med.* **60**(10), 1461–1466 (2019).
217. S. Zackrisson, S. M. W. Y. Van de Ven, and S. S. Gambhir, "Light in and sound out: Emerging translational strategies for photoacoustic imaging," *Cancer Res.* **74**(4), 979–1004 (2014).
218. F. Knieling et al., "Multispectral optoacoustic tomography for assessment of Crohn's disease activity," *New England J. Med.* **376**(13), 1292–1294 (2017).
219. M. Erfanzadeh and Q. Zhu, "Photoacoustic imaging with low-cost sources; a review," *Photoacoustics* **14**, 1–11 (2019).
220. D. Das et al., "Another decade of photoacoustic imaging," *Phys. Med. Biol.* **66**(5), 05TR01 (2021).
221. A. B. E. Attia et al., "A review of clinical photoacoustic imaging: current and future trends," *Photoacoustics* **16**, 100144 (2019).
222. B. T. Cox, J. G. Laufer, and P. C. Beard, "Quantitative photoacoustic image reconstruction using fluence dependent chromophores," *Biomed. Opt. Express* **1**(1), 201 (2010).
223. H. Singh et al., "Mapping cortical haemodynamics during neonatal seizures using diffuse optical tomography: a case study," *NeuroImage Clin.* **5**, 256–265 (2014).
224. M. D. Wheelock, J. P. Culver, and A. T. Eggebrecht, "High-density diffuse optical tomography for imaging human brain function," *Rev. Sci. Instrum.* **90**(5), 051101 (2019).
225. A. P. Gibson, J. C. Hebden, and S. R. Arridge, "Recent advances in diffuse optical imaging," *Phys. Med. Biol.* **50**(4), R1–R43 (2005).
226. W. Zhi et al., "Predicting treatment response of breast cancer to neoadjuvant chemotherapy using ultrasound-guided diffuse optical tomography," *Transl. Oncol.* **11**(1), 56–64 (2018).
227. R. Choe and T. Durduran, "Diffuse optical monitoring of the neoadjuvant breast cancer therapy," *IEEE J. Sel. Top. Quantum Electron.* **18**(4), 1367–1386 (2012).
228. F. Scholkmann et al., "A review on continuous wave functional near-infrared spectroscopy and imaging instrumentation and methodology," *Neuroimage* **85**, 6–27 (2014).
229. K. A. S. Mithun and W. Xia, "Portable and affordable light source-based photoacoustic tomography," *Sensors* **20**(21), 6173 (2020).
230. V. V. Beschastnov et al., "Current methods for the assessment of oxygen status and bio-tissue microcirculation condition: diffuse optical spectroscopy (review)," *Sovrem. Tehnol. v Med.* **10**(4), 183–194 (2018).
231. A. Curtin et al., "A systematic review of integrated functional near-infrared spectroscopy (fNIRS) and transcranial magnetic stimulation (TMS) studies," *Front. Neurosci.* **13**, 84 (2019).
232. P. Pinti et al., "The present and future use of functional near-infrared spectroscopy (fNIRS) for cognitive neuroscience," *Ann. N. Y. Acad. Sci.* **1464**, 5–29 (2018).
233. A. Pifferi et al., "New frontiers in time-domain diffuse optics, a review," *J. Biomed. Opt.* **21**(9), 091310 (2016).
234. E. E. Vidal-Rosas et al., "Evaluating a new generation of wearable high-density diffuse optical tomography technology via retinotopic mapping of the adult visual cortex," *Neurophotonics* **8**(2), 025002 (2021).
235. G. Di Leo et al., "Optical imaging of the breast: basic principles and clinical applications," *Am. J. Roentgenol.* **209**(1), 230–238 (2017).

236. F. Y. Wong et al., “Impaired autoregulation in preterm infants identified by using spatially resolved spectroscopy,” *Pediatrics* **121**(3), e604–e611 (2008).
237. H. S. Yazdi et al., “Mapping breast cancer blood flow index, composition, and metabolism in a human subject using combined diffuse optical spectroscopic imaging and diffuse correlation spectroscopy,” *J. Biomed. Opt.* **22**(4), 045003 (2017).
238. I. Fredriksson and M. Larsson, “On the equivalence and differences between laser Doppler flowmetry and laser speckle contrast analysis,” *J. Biomed. Opt.* **21**(12), 126018 (2016).
239. H. Jonasson et al., “Oxygen saturation, red blood cell tissue fraction and speed resolved perfusion - a new optical method for microcirculatory assessment,” *Microvasc. Res.* **102**, 70–77 (2015).
240. W. Heeman et al., “Clinical applications of laser speckle contrast imaging: a review,” *J. Biomed. Opt.* **24**(08), 1 (2019).
241. Q. Fang and S. Yan, “MCX Cloud—a modern, scalable, high-performance and in-browser Monte Carlo simulation platform with cloud computing,” *J. Biomed. Opt.* **27**(8), 083008 (2022).
242. S. R. P. K. Lanka et al., “Multi-laboratory performance assessment of diffuse optics instruments: the BitMap exercise,” *J. Biomed. Opt.* **27**(7), 074716 (2022).
243. L. Di Sieno et al., “Solid heterogeneous phantoms for multimodal ultrasound and diffuse optical imaging: an outcome of the SOLUS project for standardization,” *Proc. SPIE* **11075**, 1107516 (2019).
244. L. Kagemann et al., “Spectral oximetry assessed with high-speed ultra-high-resolution optical coherence tomography Larry,” *J. Biomed. Opt.* **12**(4), 041212 (2007).
245. M. J. Casper et al., “Capillary refill—the key to assessing dermal capillary capacity and pathology in optical coherence tomography angiography,” *Lasers Surg. Med.* **52**(7), 653–658 (2020).
246. A. H. Kashani et al., “Optical coherence tomography angiography: A comprehensive review of current methods and clinical applications,” *Prog. Retin. Eye Res.* **60**, 66–100 (2017).
247. M. Liu and W. Drexler, “Optical coherence tomography angiography and photoacoustic imaging in dermatology,” *Photochem. Photobiol. Sci.* **18**(5), 945–962 (2019).
248. R. Leitgeb, C. K. Hitzenberger, and A. F. Fercher, “Performance of fourier domain vs. time domain optical coherence tomography,” *Opt. Express* **11**(8), 889–894 (2003).
249. B. Povazay et al., “Visible light optical coherence tomography,” *J. Biomed. Opt.* **22**(12), 121707 (2002).
250. S. P. Chong et al., “Quantitative microvascular hemoglobin mapping using visible light spectroscopic optical coherence tomography,” *Biomed. Opt. Express* **6**(4), 1429 (2015).
251. S. Chen, J. Yi, and H. F. Zhang, “Measuring oxygen saturation in retinal and choroidal circulations in rats using visible light optical coherence tomography angiography,” *Biomed. Opt. Express* **6**(8), 2840 (2015).
252. G. J. Tearney et al., “In vivo endoscopic optical biopsy with optical coherence tomography,” *Science* **276**(5321), 2037–2039 (1997).
253. B. C. Quirk et al., “In situ imaging of lung alveoli with an optical coherence tomography needle probe,” *J. Biomed. Opt.* **16**(3), 036009 (2011).
254. H. Yabushita et al., “Characterization of human atherosclerosis by optical coherence tomography,” *Circulation* **106**(13), 1640–1645 (2002).
255. J. A. Evans et al., “Optical coherence tomography to identify intramucosal carcinoma and high-grade dysplasia in Barrett’s esophagus,” *Clin. Gastroenterol. Hepatol.* **4**(1), 38–43 (2006).
256. D. Lorenser, R. A. McLaughlin, and D. D. Sampson, “Optical Coherence Tomography in a Needle Format,” in *Optical Coherence Tomography*, W. Drexler and J. G. Fujimoto, Eds., 2015th ed., Springer, Switzerland (2015).
257. S. Song, J. Xu, and R. K. Wang, “Long-range and wide field of view optical coherence tomography for in vivo 3D imaging of large volume object based on a kinetic programmable swept source,” *Biomed. Opt. Express* **7**(11), 4734 (2016).
258. M. Ulrich et al., “Dynamic optical coherence tomography in dermatology,” *Dermatology* **232**(3), 298–311 (2016).

259. H. Liang et al., “Optical coherence tomography for art conservation and archaeology,” *O3A Opt. Arts Archit. Archaeol.* **6618**, 661805 (2007).
260. X. Qi, M. V. Sivak, and A. M. Rollins, “Optical coherence tomography for gastrointestinal endoscopy,” in *Optical Coherence Tomography Technology and Applications*, 2nd ed., W. Drexler and J. G. Fujimoto, Eds., pp. 1047–1081, Springer International Publishing, Switzerland (2015).
261. G. J. Tearney et al., “Imaging coronary atherosclerosis and vulnerable plaques with optical coherence tomography,” in *Optical Coherence Tomography Technology and Applications*, W. Drexler and J. G. Fujimoto, Eds., 2nd ed., pp. 2109–2130, Springer, Berlin, Heidelberg (2015).
262. K. Liang et al., “Tethered capsule en face optical coherence tomography for imaging Barrett’s oesophagus in unsedated patients,” *BMJ Open Gastroenterol.* **7**(1), e000444 (2020).
263. Z. Hosseinaee, J. A. Tummon Simmons, and P. H. Reza, “Dual-modal photoacoustic imaging and optical coherence tomography [review],” *Front. Phys.* **8**, 1–19 (2021).
264. H. Jonasson et al., “Validation of speed-resolved laser Doppler perfusion in a multimodal optical system using a blood-flow phantom,” *J. Biomed. Opt.* **24**(9), 095002 (2019).
265. K. F. Ma et al., “Laser Doppler flowmetry combined with spectroscopy to determine peripheral tissue perfusion and oxygen saturation: a pilot study in healthy volunteers and patients with peripheral arterial disease,” *J. Pers. Med.* **12**(6), 853 (2022).
266. G. Wang et al., “Impact of local thermal stimulation on the correlation between oxygen saturation and speed-resolved blood perfusion,” *Sci. Rep.* **10**, 183 (2020).
267. A. Pellicer et al., “The SafeBoosC phase II randomised clinical trial: A treatment guideline for targeted near-infrared-derived cerebral tissue oxygenation versus standard treatment in extremely preterm infants,” *Neonatology* **104**(3), 171–178 (2013).

**Michaela Taylor-Williams** received her BSc (Honours) degree in electrical and electronic engineering science from the University of Western Australia in 2018. She subsequently secured a Sir John Monash Foundation Scholarship and Cambridge Trust Scholarship to undertake her PhD at the University of Cambridge, where she is developing compact biomedical optical imaging systems for imaging tissue vasculature in microscopy and endoscopy configurations.

**Graham Spicer** received his PhD in chemical engineering from Northwestern University in 2019 and a postdoctoral fellowship at Harvard Medical School focused on advancing the state of the art in optical coherence tomography. He is currently a postdoctoral research fellow at the University of Cambridge, developing new hyperspectral and depth-resolved endoscopic imaging tools for early cancer detection.

**Gemma Bale** received her PhD in biomedical optics from University College London, pioneering broadband near-infrared spectroscopy as a tool to monitor metabolism in brain injury. Following her postdoctoral research, expanding these efforts to clinical application, she started her laboratory at the University of Cambridge where she is the Gianna Angelopoulos Lecturer in medical therapeutics in the Departments of Physics and Engineering.

**Sarah E. Bohndiek** received her PhD in radiation physics from University College London in 2008 and then worked in both the UK (at Cambridge) and the United States (at Stanford) as a postdoctoral fellow in molecular imaging. She joined the University of Cambridge in 2013 and is currently a professor of biomedical physics in the Department of Physics, the Cancer Research UK Cambridge Institute. Her team uses multispectral imaging methods to study cancer evolution.